Report No. NW/SSD/RR/42/79

Central Electricity Generating Board
NORTH WESTERN REGION

THE EFFECTS OF COMPRESSIVE STRESS ON THE ULTRASONIC RESPONSE OF STEEL-STEEL INTERFACES AND OF FATIGUE CRACKS

by

A.B. Wooldridge,
Non-Destructive Testing Applications Centre.

Date: April, 1979

Job No. ZE 372

CEGB UNCLASSIFIED

REPORT

NW/SSD/RR/42/79

SUMMARY SHEET

TITLE THE EFFECTS OF COMPRESSIVE STRESS ON THE ULTRASONIC RESPONSE OF STEEL-STEEL INTERFACES AND OF FATIGUE CRACKS

BY A.B. Wooldridge, Non-Destructive Testing Applications Centre

TO Controller of Research

APPROVED M.J. Whittle
Section Head, N.D.T. Applications Centre

DATE:	April 1979
JOB NO.	ZE 372
'SPIC' CAT. NO.	
TECH. HEAD	
PAGES	23
FIGURES	35

SUMMARY

The influence of compressive stress on the reflection and transmission of ultrasound has been investigated for machine-ground steel-steel interfaces and a fatigue crack. Using two steel blocks which were pressed together, measurements were carried out at normal incidence for a range of frequencies using both shear and compression waves.

A fatigue crack was produced by tension-tension fatiguing of a steel specimen, and the ultrasonic response was investigated for a range of static compressive loads. Through transmission measurements were made using pairs of probes of 45°, 60°, 70° angles at 2MHz and 5MHz for average stresses up to 90MNm^{-2}. The pulse-echo response of the crack was also investigated for a similar range of stresses.

CONCLUSIONS

1. Compressive stresses generally decrease the amplitude of the echoes obtained from fatigue cracks and the change may be as much as 12dB in severe cases.

2. Techniques using echo amplitudes for sizing defects are already suspect. They are likely to be inaccurate if compressive stresses exist.

3. In any situation where compressive stresses exceeding 15 MNm^{-2} can occur, the accuracy of ultrasonic transmission tests will be severely degraded.

RECOMMENDATIONS

1. When specifying threshold recording levels for automatic in-service ultrasonic inspections or the amplitude at which defect echoes are considered significant during manual inspections, one should allow for the effects of possible compressive stresses. This report indicates the magnitudes of the effects which are to be expected.

2. When testing critical components, one should consider altering the external loading conditions so as to reduce the compressive stresses in the region being inspected.

(The conclusions and recommendations are expanded at the end of the report).

CIRCULATION LIST

(F = FULL REPORT, S = SUMMARY),

HEADQUARTERS

F&S Reports Library, H.Q.

Research Division

F Director General, Research Division,
F Mr. R.B. Hill
F Dr. R. Shipp,
S Divisional Secretary,

G.D.C.D.

S Director General,
S Deputy Director General,
F Mr. H.B. Cochrane,
F Mr. M. Gemmill
F Mr. G.D. Branch,
F Mr. W. Kemmish,
F Mr. P. Bolt,

Engineering Services

F G.R.O. Shaw, NNDTU, Leeds,

NORTH WESTERN REGION

F Director General,
F Controller of Scientific Services,
F Research Manager, (2)
F Section Head, NDT Applications Centre,
F Section Head, Fracture Mechanics,
F Section Head, Automation and Control,
F Manager, Metallurgy and NDT Services,
F Mr. K. James,
F Mr. H.L. Carson (via Section Head - N.D.T. Developments),
F Mr. A.B. Wooldridge
F Dr. J.M. Coffey
F Dr. J.R. Tomlinson
F Mr. J.A. Deane
F&S Library,

N.E. REGION

S Controller of Scientific Services,
F Dr. M. Jagger, S.S.D.
F Dr. A. Lichnowski, S.S.D.
F Mr. J. Kenny, Engineering Dept.,
F&S Library,

MIDLANDS REGION

S Controller of Scientific Services,
F Mr. R.H. Robins, S.S.D.
F Mr. I. Graham, Engineering Dept.,
F&S Library,

S.W. REGION

S Controller of Scientific Services,
F Mr. P. Johnson,
F&S Library,

S.E. REGION

S Controller of Scientific Services,
S Director of Engineering,
F Mr. D.H. Turner, Bankside House,
F Mr. G. Alderman, Engineering Dept., Littlebrook,
F&S Library,

M.E.L.

S Director,
S Dr. L.A. Mitchell,
S Dr. B.A. Tozer,
F Mr. M.J. Little,
S Research Planning Officer,
F&S Library,

B.N.L.

S Director,
S Research Planning Officer,
F Mr. N. Haines,
F&S Library,
F Mr. D.R. Langston

C.E.R.L.

S Director,
S Research Planning Officer,
S Dr. W.S. Jones,
F&S Library,

S.S.E.B.

F&S Library (4),
F Mr. F. Darroch (East Kilbride),
F Mr. A. Ellor, (" "),
F Dr. Platt, (" "),

EXCHANGE AGREEMENTS AND CONTRACTS

F N.I.E.S. Mr. W.J. Adair,
F E.S.B.I. Mr. W.F. Lang,

F EPRI (2))
F T.V.A.) Via Research Programme Coordinator
F Ontario Hydro)
F Canadian Welding Institute, Via Research Manager, N.W. Region,
F Mr. R.W. Urie, SECV,

NON-C.E.G.B.

F Dr. A. Chitty, NEI Power Engineering,
F Dr. J.M. Farley, Babcock and Wilcox, Renfrew,
F Dr. P. Greenfield, GEC Turbo Generators, Whetstone,
F Mr. J. Johnson, GEC Turbo Generators, Trafford Park,
F Mr. I.P. Bell, RNPDL, Risley,
F Mr. B.S. Gray, " "
F Mr. R. Sharpe, AERE, Harwell.
F Mr. T. Jessop, Welding Institute Abindon, Cambridge
F Mr. V. Whittaker, Aston University
F Mr. B. Watkins, RNPDL, Risley.

THE EFFECTS OF COMPRESSIVE STRESS ON THE ULTRASONIC RESPONSE OF STEEL-STEEL INTERFACES AND OF FATIGUE CRACKS

by

A.B. Wooldridge

CONTENTS

LIST OF FIGURES

SECTION 2

SECTION 3

SECTION 3 (Cont'd)

No.

1. INTRODUCTION

It has long been suspected that the ultrasonic response from cracks may be altered considerably by the application of an external stress and there is some published evidence to support this (Corbly et al. 1970; Yee et al. 1974, Chang et al. 1973). A compressive stress generally decreases the amplitude of the echoes from cracks, and increases the signal transmitted through the crack. Consequently echoes from tight cracks may not be appreciably larger than those from small inclusions, making it difficult to detect the cracks in pulse-echo. Similarly, techniques which rely on obscuration of the beam may be completely ineffective because of the appreciable transmission across the crack.

Although fatigue cracks only grow if the crack tip is in tension, there are situations where an engineering component may be subject to fatigue during service at high temperature or pressure, and yet during a shut-down the resultant stress may be compressive. (This has been clearly demonstrated in the case of gas turbine blades by Lake et al, 1975.) There is some concern that any fatigue cracks present could pass undetected because of their reduced echo amplitude under these conditions. In addition, there is an increasing need for quantitative estimates of the reliability of ultrasonics, particularly for nuclear applications. Such estimates require knowledge of both the inspection system and of the defects likely to occur (Coffey, 1978). Calculations of the detection capability depend strongly on the orientation and roughness of defects, but other variables such as the presence of compressive stress need to be taken into account in certain situations.

As indicated by Serabian and Moriarty, (1957) the minimum thickness of defect which can be detected ultrasonically depends on the impedance of the material between the interfaces. Fortunately for N.D.T. very thin solid inclusions can usually be detected because they have microcracks containing gas or a vacuum which renders them only semi-transparent. A good example of such microcracks developing in a tightly oxidised crack on subsequent heat treatment is described by Collins and Black, 1978. Similarly, tight cracks containing liquid may be detected if the liquid is prevented from completely wetting the surfaces because of surface tension. Thin cracks containing air should be detectable until the separation of the surfaces becomes immeasurably small. However large compressive stresses may bring the surfaces into very close contact making them difficult to detect ultrasonically.

This report describes a series of experimental measurements to determine the extent to which compressive stress impairs the ultrasonic detection of air-filled cracks. Two types of surface have been studied; smooth, machine-ground blocks and a high-cycle fatigue crack in mild steel.

Machine-ground blocks were chosen for the first set of measurements because the stress on the surfaces was predictable and could be made as large as 400 MNm^{-2} (26 tons in^{-2}). In addition the surface morphology was known and could be modified when necessary. The reflection and transmission coefficients were measured at normal incidence using a range of ultrasonic frequencies. Similar experiments using machine-ground surfaces have been carried out by Meyer (1974) and his findings are compared in the discussion (see Section 4). However the few results which are available from real cracks seem to be limited to small fatigue cracks in aircraft wings (e.g. Chang et al, 1973) and compressor blades (e.g. Lake et al., 1975).

We chose a high-cycle fatigue crack for the second series of experiments because it is the smoothest of metallurgical defects and therefore likely to show the largest effect on loading. Measurements of the reflection from the tip and the face of a clean, dry fatigue crack were made for a range of angles and frequencies under compressive loading. The transmission of shear waves through the middle of the crack under load was also investigated using matched pairs of angle probes.

The report has three main sections and an Appendix:-

Section 2 describes the experiments on the machine-ground blocks.

Section 3 describes the growth of the fatigue crack and the subsequent measurements made on it.

Finally, in Section 4 we discuss the implications of these results for the ultrasonic detection of defects.

2. TRANSMISSION AND REFLECTION AT MACHINE-GROUND SURFACES

The studies in this section were of shear and compression waves at normal incidence only, the shear waves being produced using shear wave delay line plates. Section 2.1 reviews the theory of ultrasonic transmission through the very thin gaps between two solids, which is fundamental to the detection of defects. Section 2.2 describes the experimental arrangement, while Section 2.3. explains the calibration procedure used to calculate the reflection and transmission coefficients. Details of the results obtained for compression waves and shear waves with clean surfaces are given in Section 2.4 and 2.5 respectively. Finally Section 2.6 considers the effect of rough or corroded surfaces on the reflection and transmission.

2.1. The Transmission of Ultrasonic Waves Through a Parallel-sided Gap

It is appropriate at this stage to consider those factors which influence the detectability at normal incidence of thin planar defects in solids, and we will show that this depends primarily on the ratio of the acoustic impedances of the defect and the parent material. Kinsler and Frey (1967) give an expression for the transmission coefficient through a gap of thickness x between media 1 and 3:-

$$T = \frac{2Z_3}{\left[(Z_1+Z_3)^2 \cos^2 k_2 x + \left(Z_2 + \frac{Z_1 Z_3}{Z_2}\right)^2 \sin^2 k_2 x\right]^{\frac{1}{2}}} = \frac{P_3}{P_1} \qquad \text{Eqn. 1}$$

where P_1 = initial pressure in first medium,

P_3 = pressure in third medium,

Z_1, Z_2, Z_3 are the acoustic impedances,

and $K_2 = \frac{2\pi}{\lambda_2}$ = wave number in medium 2.

In our case of a uniform parent material, $Z_1 = Z_3$ and so eqn. 1 becomes

$$T = \frac{1}{\left[1 + \tfrac{1}{4}\left(\frac{Z_2}{Z_1} - \frac{Z_1}{Z_2}\right)^2 \sin^2 k_2 x\right]^{\frac{1}{2}}} \qquad \text{Eqn. 2}$$

cf. Krautkramer J. 1977. p. 27.

This indicates that the transmission will vary periodically, being a maximum for $k_2 x = 0, n\pi$ where n is an integer.

i.e. when $x = 0, \frac{\lambda}{2}, \lambda, \frac{3\lambda}{2}$ etc.

However in the case of an air-filled gap in steel, $\frac{Z_1}{Z_2}$ is extremely large so that the transmission peaks are very narrow. In practice an air gap in steel only transmits appreciably as x tends to zero. The transmission coefficient T equals 0.7, giving an energy transmission of 50% when

$$\tfrac{1}{4}\left(\frac{Z_2}{Z_1} - \frac{Z_1}{Z_2}\right)^2 \sin^2 k_2 x = 1.$$

When $\frac{Z_1}{Z_2} \gg 1$, $\sin^2 k_2 x = 4\left(\frac{Z_2}{Z_1}\right)^2$

or $x = \left(\frac{Z_2}{Z_1}\right) \frac{\lambda 2}{\pi}$.

For a steel-air-steel interface $Z_{2/Z_1} = 7.1 \times 10^{-6}$

and for a 1MHz compression waves $\lambda_2 = 330\mu m$,

giving $x = 7.5 \times 10^{-4} \mu m$.

Because of the limitations on flatness and parallelism of the steel surface they would, in practice, be in contact before any transmission occurred.

In the case of a liquid-filled gap, however, the separation required for 50% transmission of energy is 15μm, whereas for a thin slag inclusion with $Z_{2/Z_1} = 0.34$, 50% transmission occurs for a thickness of about 0.8 mm (Szilard, 1967).

2.2. Experimental Details

Two mild steel blocks 90 mm in diameter were machined as shown in Fig. 1. The contact surfaces AB were machine-ground to a finish of 8μin Ra (0.2μm Ra) which was measured using a Surtronic surface profile meter. Recesses C and D were made to hold the piezoelectric crystals. Compressive loads were applied to the faces EF and GH using a Denison hydraulic test machine. To achieve a high stress on the contact surface, the diameter of the contact surface AB was less than the outside diameter of the blocks; a maximum stress of about 400 MNm^{-2} could be achieved. Before each set of measurements, the contact surfaces were carefully cleaned with a degreasing agent. The piezoelectric crystals were fixed directly to the steel blocks using electrician's solder. Because of this, they were well damped and the frequency response was wideband. The frequency of operation could be altered slightly by changing the frequency of the sine wave transmitter, but to obtain a wider range, or for shear waves,

it was necessary to change the crystals. Each crystal was chosen so that the contact face AB lay in the ultrasonic far field and so that the 20 dB beamwidth was considerably narrower than the contact area.

Various transducer excitation waveforms were investigated, including single cycle sine waves and long sine wave bursts. However, the length of the excitation pulse had little effect on the measured reflection or transmission coefficients, providing that the frequencies chosen were relatively close to the resonant frequency of the crystal. All the results quoted in Section 2 were obtained using a four cycle sine wave burst from a Tektronix FG 504 Function Generator. This has a fixed output impedance of 50 ohms and the input impedance of the receiver amplifier was also arranged to be 50 ohms.

The use of separate transmitter and receiver amplifiers also enabled cross-talk between the transmit and receive channels to be eliminated. Because the transit times for the reflected and transmitted signals are identical, cross-talk from the large reflection signal swamped the minute transmission signal at low loads when the same module was used for transmission and reception. The amplitude of the unrectified r.f. signals was measured either directly using an oscilloscope or else using a boxcar system to sample the peak of the waveform.

Typical results for the transmitted and reflected signals using 2MHz compression waves are shown in Figs. 3(a) and 3(b) respectively. Whereas the transmission flattens off at the highest stresses, the reflection still appears to decrease although less rapidly than at low stresses. There is a noticeable difference between the curves for increasing and decreasing load and this effect is discussed in Section 2.3.

2.3. Calibration Procedure for the Calculation of Transmission and Reflection Coefficients

The amplitude reflection coefficient for a boundary is defined as the ratio of reflected ultrasonic amplitude to incident amplitude actually at that boundary. Consequently absolute measurement of the reflection coefficient by a probe remote from the boundary must involve knowledge of how the beam spreads on travelling between the probe and the boundary. Fortunately since the reflection at a steel-air interface is unity for all practical purposes, this provides a reference point for the reflection at zero load. All the measurements for reflection under stress can then be related to this value.

The measurements of transmission coefficient depend on the sensitivities of each probe and on the beamspread. However, since the blocks are symmetrical (see Fig. 2), the path difference and the beamspread are the same in transmission as in reflection. Providing that the transmitting and receiving crystals are similar, and that the impedances of the driving and receiving circuits are the same, we can relate the transmission and reflection coefficients. It will be shown below that the relative sensitivity of the transmission system is equal to the geometric mean of the pulse-echo sensitivities of the individual probes.

To develop this mathematically, let V_{AA} and V_{BB} be the echo amplitudes for crystals A and B respectively, acting in pulse-echo under a specified load. Also let V_{AB} be the amplitude of the signal transmitted from A to B under the same load. Then $V_{AB} = V_{BA}$ by the Reciprocity Theorem (Hueter and Bolt, 1966), providing that the impedances of the driving and receiving circuits are similar. This was also confirmed by experiment. But

$$V_{AA} = t_A \, f(2D) \, r_A . \, R \qquad \text{Eqn. 3}$$

where t_A = transmitting sensitivity of A

r_A = receiving sensitivity of A

R = reflection coefficient at the interface

and f(2D) is a factor allowing for the beamspread at range 2D.

Similarly, $V_{BB} = t_B \, f(2D) \, r_B \, R$ Eqn. 4

and $V_{AB} = t_A \, f(2D) \, r_B \, T = t_B \, f(2D) r_A \, T$ Eqn. 5

where T = transmission coefficient at the interface.

$$\therefore \quad \frac{(V_{AB})^2}{T^2} = \frac{V_{AA} \, V_{BB}}{R^2} \quad \text{from equations 3, 4 and 5.}$$

or $$\frac{T}{R} = \frac{V_{AB}}{\sqrt{V_{AA} V_{BB}}} \qquad \text{Eqn. 6}$$

Equation 6 shows that by measuring the pulse-echo signals for each crystal and the transmission signal, the transmission and reflection coefficients may be compared directly. To make the transmission and reflection signals equivalent, the transmission signals are divided by the geometric mean of the pulse-echo sensitivities. Both sets are then scaled equally so that the reflection coefficient is unity at zero load. This procedure has been used to calculate the transmission and reflection coefficients for all the measurements made using the ground steel blocks.

Fig. 4 shows the two coefficients for 2 MHz compression waves. In media of constant impedance the energy reflected or transmitted is equal to the square of the appropriate amplitude coefficient. The maximum value of the transmission amplitude is 0.96 which corresponds to reflected energy of 92%. Similarly the reflection coefficient is 0.23 which corresponds to 5% energy reflected. The apparent loss of 3% of the energy is not significant because the accuracy of measuring the transmission coefficient is estimated to be $\pm$5%. The most important errors are likely to be caused by slight misalignment of the transmitting and receiving crystals. Since the calibration technique assumes that the transmitter and receiver are accurately aligned, if this is not the case the transmission readings will be reduced relative to the pulse-echo readings.

We also investigated the possibility of further energy loss by mode conversion to surface waves. This was done by placing a steel plate between the pole pieces before compressing them (see Fig. 5). A surface wave probe was placed on the top surface of the steel plate and the magnitude of the surface waves recorded as the load increased. Although it was not possible to measure the total energy present in the surface waves, the surface waves were load dependent and their amplitude decreased by 6dB when the stress was increased from zero to 3 tons in^{-2}. The implication is that some energy is lost as surface waves, but this becomes less serious at higher stresses.

2.4. Measurements using 2, 4 and 6 MHz Compression Waves

We have already referred to Figs. 3(a) and 3(b) which show the transmitted and reflected signals as a function of stress on the surfaces for 2MHz compression waves. Readings were taken with the load increasing and then decreasing. In particular, the reflected signal is less by up to 30% during the unloading cycle. We attribute this to local plastic deformation of the contact surfaces during the loading cycle which improves the ultrasonic transmission. This hysteresis effect was investigated by repeated cycling of the blocks, but the load was never reduced to zero during intermediate cycles so as to prevent relative movement of the blocks. Fig. 6(a) shows the result of two complete cycles; the reflected amplitude fell after the first loading cycle, but remained fairly constant thereafter.

For subsequent measurements a more reliable method was sought for fixing the two blocks together to prevent relative slip, so the blocks were held with three thin metal straps tack-welded between the blocks. Because of the residual compressive stress induced by welding on these straps, the transmission under zero load was increased to 30 per cent of the maximum value. (This would correspond to a compressive stress of about 30 MNm^{-2}). Fig. 6(b) shows the reflected amplitude for two complete cycles and as in Fig. 6(a), the reflection drops after the very first load cycle, but is then insensitive to further cycling. Again a likely explanation of this hysteresis is that the surfaces deformed under the very first loading so as to mate closely. Subsequent changes in load below the highest value previously applied produce only elastic deformation of the blocks which is reversible.

The 2MHz crystals which had been used for the previous experiments were replaced with 10mm diameter PC5 crystals which, though nominally 5MHz, could be driven at 4MHz and 6MHz. These were soldered to the blocks as described in Section 1.1 and the two blocks were pinned together with tack-welded straps as before. Five complete loading cycles were measured, but as observed at 2MHz the ultrasonic responses over all cycles after the first were practically identical. Finally, the welded straps were removed to eliminate any residual compressive stress, and readings were repeated over one loading cycle.

The reflected and transmitted signals were generally similar to those obtained at 2MHz. To aid comparison, Fig. 7 shows the reflection and transmission coefficients for 2, 4 and 6MHz compression waves. As predicted by equation 2 in the introduction, waves of higher frequency have lower transmission coefficients, and as one might expect the reflection coefficients are higher. The frequency dependence is seen to be small, and for all frequencies the biggest changes in reflection and transmission occur during the first 80 MNm^{-2} (5.2 tsi) of loading.

2.5. Measurements using 1MHz and 4MHz Shear Waves

Since most ultrasonic testing is carried out using shear waves, it was necessary to investigate the stress dependence of their transmission and reflection coefficients to see if they showed the same behaviour as compression waves.

Shear wave, ultrasonic delay line crystals 8 mm square, of nominal frequency 5MHz were attached to the steel blocks using Eccobond 50C silver epoxy paint. This produced a rigid bond after curing at 100°C for 2 hours, yet could be removed relatively easily with solvent and proved more convenient than solder with these crystals. Four-cycle sine wave pulses at either 1MHz or 4MHz were used to excite the crystals. Since shear wave crystals produce linearly polarised beams, these were brought into the correct orientation by rotating the blocks relative to each other until the transmitted signal attained its maximum value.

The transmission and reflection amplitude coefficients calculated using eqn. 6 of Section 2.3. are shown in Fig. 8 for the 1 MHz and 4 MHz shear waves. The lower frequency waves were transmitted better, the maximum transmission for a loading of 300 MNm^{-2} (20 tons in^{-2}) being 0.89 for 1MHz and 0.84 for 4MHz. Similarly the lower frequencies were reflected less strongly under stress, the reduction in reflection being 10dB for 1MHz and 6dB for 4 MHz. Fig. 9 summarises the reflection results so far and shows on a logarithmic scale how the reflection coefficient depends on the wave mode, frequency and applied stress. Note that the decrease in reflected amplitude never exceeds 12dB for compressive loads of 300 MNm^{-2} (20 tons in^{-2}). Shear waves are transmitted less than compression waves of the same frequency and this may be partly because the wavelength of shear waves is roughly half that of compression waves of the same frequency. It should be remembered, however, that the detailed interactions at the surface which gives rise to the transmission or reflection are fundamentally different in the cases of shear and compression waves.

2.6. The Dependence of Ultrasonic Transmission on the Nature of the Interface

At low stresses, the ultrasonic transmission coefficient is particularly sensitive to changes in the stress applied to the surfaces. The results of Sections 2.3 and 2.4 have shown that whereas the transmission at zero load is immeasurably small, it increases rapidly for small loads. A transmission coefficient of 0.1 is easily measurable, whereas the corresponding reflection coefficient at the same load would be about 0.99 which is difficult to distinquish from the zero load value of unity. Similarly we expect the transmission coefficient to be much more sensitive to the morphology of the surfaces at low stresses.

Kendall and Tabor (1971) showed that the ultrasonic transmission across an interface is proportional to the elastic stiffness, which is defined as the ratio of stress to incremental displacement at the interface. This stiffness depends on the number of microscopic points of contact and their distribution, and not just on the integrated area of contact. In particular, when the contact area between the interfaces is less than one tenth of the apparent area, the transmission should be proportional to the square root of the true contract area.

2.6.1. Steel Wool Inserted Between the Contact Faces

To investigate the effect of varying contact area, pads of steel wool of varying thickness, made of 50 m diameter wire, were placed between the blocks which were compressed in the Denison hydraulic machine . The actual area of contact of the steel wool was estimated by measuring the optical transmission through the pads which were recovered after the compressed blocks had finally been unloaded.

In Fig. 10 the ultrasonic transmission of three steel wool pads is compared with that of the ground blocks for 4MHz compression waves. Taking the percentage of optical obscuration as a measure of the area of contact, A_c, the ultrasonic transmission at maximum stress is seen to vary relatively little with increasing contact area. Fig. 11 lists the transmission coefficients for each pad and there is some indication that the transmission is related to the square root of the contact area. These results also indicate that even non-mating surfaces might allow appreciable transmission under modest loads. For example, pad 3 which was 200μm thick after compression, had a transmission coefficient of 0.6 for a macroscopic applied stress of 80 MNm^{-2} (5 tons in^{-2}).

2.6.2. Corroded Contact Faces

Since many components operate in corrosive environments, any surface-breaking cracks are liable to be filled with oxides, or other products of corrosion. The nature of such corrosion depends strongly on the physical conditions and the kind of contaminants present at the crack. However as an example, the corrosive effect of warm chlorinated water was simulated by immersing the blocks in a bath of synthetic sea water at 80°C for 12 hours. Prior to the corrosion, the blocks were fixed rigidly together with tack-welded pins as before, and the welds were arranged to produce only a small stress on the contact faces (~ 15 MNm^{-2}). The piezoelectric crystals were left in position on the block during the corrosion process so that readings before and after would be directly comparable. After aqueous corrosion, the crack faces were thoroughly dried.

Fig. 12 compares the transmitted and reflected signals for clean, ground surfaces and corroded surfaces obtained with 2.5 MHz compression waves. At high stresses the transmission is lower for the corroded surfaces and the reflection is higher, as one might expect. However at low stresses, the transmission is higher for the corroded surfaces which may indicate that in some places, a tight bond is formed between the metal surfaces, thus allowing better transmission than in the case of the ground blocks.

On separating the two blocks, we found that the oxide film was not uniformly thick, but was thicker around the outside of the contact area. Consequently one must be cautious in interpreting these limited results since the oxide may have prevented proper contact of the surfaces in the centre of the beam path. A very wide range of corrosion processes may occur in practice and subtle changes in the oxide structure may produce large changes in the ultrasonic response. Consequently, a firm statement of the effect of corrosion in any particular situation must depend on measurements made on a reasonable number of specimens corroded under carefully controlled conditions similar to those experienced in the practical situation.

3. THE SHEAR WAVE RESPONSE OF A LARGE FATIGUE CRACK UNDER COMPRESSION

In contrast with the simple geometry and controlled surface condition of the ground blocks, real cracks often have irregular geometry and the surface morphology depends on the crack growth conditions. In particular the material in the region of the crack tip may have been plastically deformed, making it very difficult to predict the stress state at the crack tip. The fatigue crack used for these experiments was made large so that transmission measurements would not be influenced by the edges of the crack. In addition the crack tip was kept as straight as possible to simplify interpretation of the scattering from the region close to the tip.

3.1. Description of the Specimen

3.1.1. The Growth of the Fatigue Crack

A block of BS15 mild steel 50 mm thick was cut and machined as shown in Fig. 13 and checked for laminations and other defects using a compression wave probe at high gain. A few small, isolated defects were detected along the centre line of the block, but they were not close to the line of the crack and unlikely to cause serious problems.

The block was supported in a hydraulic test machine by the holes A and B, and a fatigue crack grown in the direction XY. The block was essentially a compact-tension or wedge-opening-load type specimen whose length had been extended so that 70° shear wave probes could be used to study an appreciable length of the crack. To prevent deviation of the line of the crack and to maintain a uniform growth rate along the crack tip, a groove of semi-circular cross-section was machined in the sides of the block along XY. Also a slot was spark-eroded along the 50 mm thickness at X to aid initiation of the fatigue crack. The face CD was ground smooth so that ultrasonic probes could be easily scanned along the surface to measure the response of the crack.

At the beginning of the crack growth a change in stress intensity factor Δk of 25 $MNm^{-3/2}$ was imposed, giving a growth rate of about 5mm/hour at 10Hz cycling rate. The ratio of minimum to maximum stress, the R-factor, remained constant at 0.04. The crack growth rate was monitored with an optical microscope and also using dry magnetic particle detection; the latter was generally found to be more convenient. During the early stages, the crack grew more slowly on one side than the other; this was because of slight misalignment of the jaws. Consequently the orientation of the block in the jaws was reversed at regular intervals to maintain equal growth rates at either side of the crack. About 100,000 fatigue cycles were necessary to initiate the crack, and after a further 230,000 cycles the crack had grown to 31 mm. Since the stress intensity factor had by then increased to about 70 $MNm^{-3/2}$ and the crack growth was becoming difficult to control, the load amplitude was adjusted to reduce the change in stress intensity factor to about 50 $MNm^{-3/2}$. A further 7000 cycles brought the crack to its final length of 37mm. Subsequent destructive examination revealed that the sudden change in loading conditions when the crack was 31 mm long had produced a marked reduction in the roughness of the crack surfaces at this point.

3.1.2. Results of final destructive examination

When all experiments on the block had been completed, it was split open by freezing in liquid nitrogen and hitting it sharply so that it broke by brittle fracture (see Fig. 14(a)). The final dimensions of the crack, which are

shown in Fig. 15(a), were very close to those measured by magnetic particle testing, and the line indicating the change in fatigue growth conditions was clearly visible. Although the crack was slightly longer on one side of the block than the other, the crack tip was remarkably straight and appeared from the changes in roughness to have remained so for most of the growth. Light corrosion had occurred along this line, whereas the main part of the crack was very clean. Because corrosion had only occurred along a line, it is attributed to the contrast paint used prior to the magnetic particle inspection. The paint was applied just before the load amplitude was reduced, and the freshly exposed surfaces presumably experienced the most rapid corrosion.

The roughness of the crack, measured using a Surtronic 2 roughness meter with the cut-off set to 0.1 inches, was found to increase steadily from 7μm Ra at the start to about 17μm Ra at the point where the load amplitude was reduced (see Fig. 15(b)). The correlation length of the roughness was measured by connecting the analogue output of the Surtronic 2 to a 3721A Hewlett Packard Correlator. This correlation length was found to increase from 0.10 mm to 0.14 mm from the start of the crack to the region of maximum roughness.

The crack roughness is compared with the theoretical growth rate per fatigue cycle in Fig. 16. Fracture mechanics predicts that the growth rate per cycle $\frac{da}{dn}$ is given approximately by:-

$$\frac{da}{dn} = 10^{-11} (\Delta k)^3 \text{ m/cycle} \qquad \text{Eqn. 7}$$

where the change in stress intensity factor Δk is given by

$$\Delta k = \frac{(P_{max} - P_{min})\, Y}{BW^{\frac{1}{2}}}$$

P_{max} and P_{min} are the maximum and minimum loads, while Y, B and W depend on the geometry of the block.

Fig. 16 only shows the predicted growth rate for the first 25mm of the crack because the assumptions on which eqn. 7 is based are not valid for very large values of the geometric compliance factor (Y) and fracture mechanics tables of Y run out at this point.

Examination of the crack surface using an electron microscope revealed that in addition to the increase in roughness towards the crack tip, small cracks existed in the areas of maximum roughness. These cracks were as long as 0.5 mm as seen in Fig. 14(b), but it was not possible to measure their depth. In general they appeared to be perpendicular to the main surface of the crack.

3.2. B-Scan Displays of the Fatigue Crack under Zero Load

A wide range of ultrasonic probes was used to make measurements on the fatigue crack and the main characteristics of these probes are listed in Fig. 17. All these probes were checked before use with a Metrotek A101 ultrasonic Pulse-Receiver to obtain records of the pulse length, and for the B-Scan probes, the beamspreads were also measured. Typical echoes from a standard reflector for probes of types 1 and 2 are shown in Fig. 18.

Prior to fatiguing, B-scans were recorded for the central region of the block in which the crack was to be grown, using 45°, 60° and 70° angled

shear wave probes on the face DC. Some ultrasonic readings were taken during the growth of the crack, but as mentioned before, we relied on magnetic particle detection for measuring the growth rate. After fatiguing, magnetic particle tests indicated a crack-free ligament of 26mm while various ultrasonic tests indicated a ligament of between 24 and 27 mm. As described in Section 3.1, destructive examination showed that the ligament actually varied from 23 to 25 mm (see Fig. 15(a)).

Fig. 19(a) is a B-Scan photograph obtained with a 60° 5MHz shear wave probe when the crack was fully grown. The geometry of the block is shown in Fig. 19(b) which also indicates by dotted lines the echoes from the starter notch and from the fatigue crack itself. Echoes caused by multiple bounces of the ultrasonic beam in the side arms are plotted on the B-Scan at the appropriate range, but along the beam axis of the probe. There is a considerable number of possible bounces, and they all give rise to indications in the B-Scan which lie behind the line of the crack. For a 60° probe, the first 10mm of the crack surface were always too smooth to produce an echo above the B-Scan threshold.

Fig. 20(a) is a B-Scan photograph for a 70° shear wave probe. As in Fig. 19(a) the crack appears to be curved near its tip, but this apparent curvature is caused by the beamspread of the probe since the effect is reversed when the crack is imaged in the opposite direction. A higher gain is needed to display the crack near its open end, and although the range is increasing, the echo drops off more rapidly than one would predict for a crack of uniform roughness. We have already remarked on the similar but more extreme behaviour of the echoes for a 60° probe. In addition, the 70° B-Scan in Fig. 20(a) indicates a change in the crack topography as a depth of 30mm below the top surface CD. This is consistent with the crack growth conditions since the loading amplitude was reduced when the uncracked ligament was 29mm deep, and destructive examination confirmed these indications. (see Section 3.1.2.). Fig. 20(b) shows the corresponding B-Scan photograph for a 45° probe which reveals clearly only the region near the crack tip. When the gain was increased still further, internal echoes swamped the signal from the crack tip before the smoother part of the crack became visible.

So far, ultrasonic beams had been directed at the crack only from the face CD. To allow a wider response of the crack tip to be measured, face EF was prepared by cutting off the side arms along the line GH in Fig. 13 and grinding the surface. This allowed measurement both of the crack echo response from the bottom surface and for the transmission of shear waves through the crack from one face to the other. For completeness, Fig. 21 shows a series of 60° B-Scans of different sensitivities taken from the surface CD after removal of the side arms. The multiple reflections in Figs. 19 and 20 are no longer present, but there are pronounced corner echoes from the starter notch, which appear just behind the main echo from the curved part of starter notch. Fig. 21(a) shows the echo from the crack tip (24 mm below the surface) together with an apparently small scatterer just below it, which corresponds to the roughest part of the crack (30 mm below the surface). It is these two distinct echoes which were used for the majority of the subsequent reflectivity experiments. Figs. 21(b) and (c) which were taken at higher sensitivity reveal further fine structure along the crack.

Figs. 22(a) to (c) are 60° B-Scans taken from the lower surface EF, while Fig. 22(d) is a 70° B-Scan taken at high gain. The 60° B-Scans show that as the sensitivity is increased more of the crack becomes visible. In addition there is a very pronounced mode conversion echo which gives a line on the

B-Scan at about 30° to the crack; the origin of this is shown in Fig. 23(a). Shear waves incident on the crack at 30° to the normal undergo appreciable conversion to compression waves at nearly grazing incidence. These are reflected by the bottom surface CD and re-radiate shear waves at 33° when they interact with the crack face. Now the B-Scan always plots reflections as if they lie on the beam axis, and in this case it is calibrated in time-of-flight for shear waves. Consequently a mode conversion occurring at the point R of the surface would be plotted at the point Q such that the ratio of RQ to RT is equal to the ratio of the shear and compression wave velocities. The locus of all such points is a line at 33° to the crack as shown in Fig. 23(b) and it is this line which occurs in the 60° B-Scans. The amplitude of the mode-converted echoes is comparable in magnitude with the direct echoes from the tip or the face of the crack.

3.3. Magnitudes of the Crack Tip and Crack Face Echoes under Zero Load

The B-Scan results described in Section 3.2. had indicated that the surface of the fatigue crack did not have a mirror finish, but rather was sufficiently rough to scatter sound back to the probe even when the sound was incident at 45°. In particular, a discontinuity in the reflecting characteristic existed about 5-10 mm from the crack tip, the crack being substantially smoother between this region and the open end. To quantify these observations, the pulse-echo response of the crack was measured using a range of shear wave angle probes placed on either surface CD or EF of Fig. 23(b). In the case of 45° and 60° probes, an echo from the tip and an echo from the crack face could be distinguished. For 70° probes, however, the difference in range was not usually sufficient to enable the separate echoes to be clearly distinguished. Nevertheless, the measurements are treated in the following discussion as if they arose solely from the crack tip.

Fig. 24 shows the variation of the equivalent flat bottom hole (F.B.H.) size of the crack tip echo with the angle of incidence. This angle is defined as in Fig. 23(b) and varies from 30° to 135°. Results are shown for three types of 5MHz probe and one type of high resolution 2.25MHz probe of which the important parameters have been outlined in Fig. 17. Apart from the 60° and 120° readings for probe type 2, the equivalent F.B.H. sizes range from 0.7 mm to 1.2 mm. Surprisingly, the spread of readings for different angles of the same type of probe is no larger than the variation between probes of different types with the same angle of incidence; in other words the angular dependence was less than the experimental scatter. The origin of the larger echoes obtained at 60° and 120° for the 5MHz parametrics probe is not known. However, we can speculate that a combination of mode conversions and multiple scattering between tiny facets of the crack is sending sound back to the receiver and that in this case at least, the effect is most pronounced at 60°. The B-Scans in Section 3.2 also indicate that mode conversions are particularly strong for 60° probes.

The strength of the echo from the crack tip depends strongly on the squint angle of the probe, and the recorded values were the maximum signals that could be obtained. One quick measurement showed a drop of 4dB for a 5° misorientation, but this will probably depend strongly on the beamspread of the probe. If the probe were constrained to scan along parallel lines as would be the case in an automatic inspection, the recorded echo strengths would in general be lower than those shown in Fig. 24.

3.4. Transmission of Shear Waves through the Crack under Load

Turning now to transmission through the crack, it was pointed out in Section 1 that negligible transmission is likely to occur until the separation of the faces is less than about 10^{-5} mm. In practice, because of the roughness of the crack surfaces, asperities on the surface will actually be in contact before the theoretical separation of 10^{-5} mm is achieved. Consequently transmission begins when the crack surfaces first come into contact, while the rate of increase in transmission on further loading depends on the ease with which the surfaces mate together.

Transmission of shear waves across the crack at 45°, 60° and 70° was measured at 2MHz and 5MHz, the experimental arrangement being shown in Fig. 25. The table lists the positions of the transmitting and receiving probes measured from the mid-line of the block. These positions were chosen such that the beam axis intersected the crack about 18mm from the start of the crack. In this position the beam was well clear of both the starter notch and the crack tip. Pairs of Baugh & Weedon 2MHz and 5MHz angle probes were used for all the measurements. Compressive loading, up to a maximum of 88 MNm^{-2} (5.7 ton in^{-2}) was applied on the faces CF and DE using the Denison hydraulic machine. The actual stress distribution on the crack face is variable and unknown, particularly before the crack becomes fully closed; here, however, the stress used is taken as the ratio of the load applied and the total cross-sectional area of the bar (i.e. the crack plus the uncracked ligament).

Figs. 26 and 27 shows the transmitted signals for 2MHz and 5MHz shear waves at 45° to the crack; in the inset graphs we indicate on an expanded scale the variation in transmission at low loads. Negligible transmission occurs until the mean stress reaches 15MNm^{-2}; after this point the transmission increases rapidly indicating that the crack has become tight. At the maximum stress applied of 88 MNm^{-2}, the transmission at 2MHz has flattened off at a level 4dB below that through an uncracked section of the block. At 5MHz the transmission is 10dB below that transmitted through an uncracked section, but is still increasing. In each case, a slight reduction in transmission occurs at a mean stress of about 30MNm^{-2}. The measurements made with pairs of 60° and 70° probes also showed a small oscillation as the crack closed, followed by a rapid monotonic increase in transmission at higher stresses. The transmission at maximum stress for 30° incidence on the crack (60° probe) was only 1dB less than the transmission through an uncracked section 2MHz, but 9dB less at 5MHz (see Fig. 28).

We are unlikely to be able to explain oscillations in the dependence of ultrasonic response on stress in terms of a monotonically increasing stress. Therefore we have considered the changing stress distribution across the block as the crack closes to see if it is indeed a monotonic fuction of applied load. The simple linear elastic model discussed in Appendix A predicts these changes in stress distribution, and indicates that it is possible for the area of the crack face in contact to increase so quickly with load that the stress local to the crack tip is temporarily relieved. During the growth of the crack, the ligament is plastically deformed so that at zero load the crack remains open, except perhaps the crack tip itself. When a compressive load is applied, the crack tip is put in compression whereas the outer edge of the ligament is in tension. As the crack continues to close, the stress gradient along the plane of the crack is reduced. If the crack closes rapidly with increasing load, the compressive stress near the crack tip may actually decrease even though the mean stress on the block is increasing. Whereas the stress at the crack tip is reduced very rapidly as the crack closes, the stress on the middle at the

crack changes much more slowly (see Fig. A2). Since the probes are arranged to transmit mainly through the middle of the crack, the transmission measurements show smaller fluctuations than the reflection directly from the crack tip described in the next section. Evidence that the surfaces of the crack were progressively closing was provided by the 60° transmission probes. When the mean stress was about 40MNm^{-2}, the transit time of the signal decreased at the same time as the amplitude increased. This change in time-of-flight, which was equivalent to 4mm travel path, presumably indicates that whereas energy was initialy being transmitted through the region nearer the crack tip, more energy became transmitted along the line-of-sight as the crack closed.

3.5. Pulse-echo Response of the Crack Tip and Crack Face under Load

For this series of measurements, the block was supported in the Mand hydraulic test machine using steel pins in the holes P and Q of Fig. 13 so that compressive or tensile loads up to a maximum of 250 kN could be applied. For each set of measurements the probe was fixed in position on the side DC and the echo amplitude recorded as the load varied.

Fig. 29(a) shows the signal recorded with a Baugh and Weedon 5MHz, 70° probe positioned so that the beam axis passed through the crack tip. The amplitude drops sharply under compressive loading to a local minimum at about 20MNm^{-2} (1.3 ton in^{-2}), increases to a maximum at 30MNm^{-2}, and then reverts to a minimum value at stresses above 40MNm^{-2}. These stress values are close to those at which the transmission shows an oscillation (Section 3.4).

Intuitively, one would expect a more uniform stress distribution on the crack face due to compressing the face DE and CF than due to loading via the holes P and Q, since the latter do not lie along the axis of the block. The model in the Appendix confirms this view, but predicts that the difference between the two cases is not pronounced. The blocks were compressed along the end faces using a Denison hydraulic machine and, as the theory indicates, a similar oscillation in the reflectivity was again obtained. Fig. 29(b) shows that the reflectivity dropped to a minimum at 11MNm^{-2}, rose to a maximum at 26MNm^{-2} and dropped again at higher stresses.

When other probes were used to investigate the response of the crack tip and crack face, the results varied both with the type of probe and with the position at which the beam axis intersected the crack. Reflected signals from the region near the crack tip obtained with various probes are shown in Figs. 30 (a) to (c); no consistent trend appears and in some cases the echo amplitude even increased with load. Reflections from the crack face were of similar magnitude, but their load dependence was just as variable. The reason is that reflection from the crack face, and indeed from the crack tip, is very weak, and depends strongly on the fine structure of the crack surfaces; a perfectly smooth crack face would give no back-scattered echo at the non-normal incidence used in these experiments. Optical and electron mciroscope photographs of the crack surface described in Section 3.1 show that the roughest part of the crack also has microcracks which lie roughly perpendicular to the surface. Such cracks are unlikely to be closed significantly by the compressive load applied and may explain the results of Fig. 30(b) where the reflected signal is seen to

remain steady or even increase slightly with applied load.

Fig. 31 lists the maximum and minimum changes in echo amplitude from either the crack tip or the crack face which occurred at any point between zero load and the maximum stress of 90MNm^{-2} (5.8 ton in^{-2}). The average changes measured using a range of probes are also listed. The maximum variations in reflectivity with loading are comparable with those measured with the two steel blocks under similar stresses. However the response of the fatigue crack is less predictable than that of the steel blocks for the reasons outlined above.

3.6. Two-Probe Techniques

3.6.1. Detecting diffracted edge waves

The crack tip is expected to radiate approximately cylindrical edge waves, and in the final series of experiments, a separate receiver was used to measure the amplitude of such scattered waves. The transmitting and receiving probes were set up facing each other on either side of the crack as shown in Fig. 32, but with the beam axes arranged to intersect the crack tip. The signals depended strongly on the relative orientations of the probes and the crack as well as on the separation of the probes. With the probes adjusted for maximum signal, the diffracted echoes were lower than those obtained in pulse echo: 6dB less for 45° and 10dB less for 70°. Because of poor sensitivity and the dependence on probe orientation, this technique appears to be inferior to pulse echo for detecting vertical cracks. However, a similar technique has been used with considerable success to measure the depth of fatigue cracks, once detected. Lidington, Silk et al. 1976 used diffracted compression waves to size fatigue cracks because they are the first to arrive at the receiver probe.

3.6.2. Diffraction and Transmission across the Crack under load

In certain situations, rough cracks which have facets spaced by less than the beamwidth may produce an echo response which is similar to that from a line of point defects, but it is important for fracture mechanics predictions to be able to distinguish a continuous crack from a number of unconnected point defects. A probe arrangement which might achieve this in certain circumstances is shown in Fig. 32. The probes are moved so that the distance of each probe from the line of the crack is equal. Then using a "pitch-and-catch" technique, one might expect strong diffracted signals from an array of point defects, but no signal from a continuous crack other than a diffracted edge wave from the crack tip. If the crack is under compression, however, there may be considerable transmission, making it difficult to distinguish continuous cracks from arrays of point defects. This was indeed found to be the case when a compressive stress was applied to the fatigue cracks, as described below.

Since high gain was necessary to detect the diffracted signals, a separate receiver amplifier was used to prevent cross-talk between the transmission and reception channels. Fig. 33 shows the stress dependence of the diffracted signals from three points along the crack measured using pairs of Baugh & Weedon 2MHz 45° shear wave probes. At zero load, the only signal was from the crack tip, about 25mm below the surface CD. Under load, whereas the signal from the crack tip decreased by up to 19dB, signals from the crack face increased so that at a stress of 75MNm^{-2}, diffracted signals were obtained from the whole length of the crack. Apart from the crack tip, the strongest signal was obtained from a point on the crack face about 34mm below the surface CD corresponding to the roughest part of the crack (see Section 3.1.2.). This signal was as large as that from the tip at stresses above 40MNm^{-2} while that from a point 53mm below the surface was 12dB lower.

This trend can be explained as follows. When the crack faces are not in contact, only the tip scatters signals to the receiver. Under load, some of the asperities at the tip become tight, and so the crack presents less of a discontinuity to the beam. Consequently the diffracted signal from the tip is weaker since more energy passes straight through. Meanwhile small areas at the crack face make contact and cause sound to be diffracted through the crack to the receiver.

4. DISCUSSION OF RESULTS

The measurements of reflection and transmission coefficients for the ground steel blocks have shown how the coefficients vary rapidly over the first 100 MNm^{-2} of loading, but for these blocks the reflection coefficient never dropped below 0.25 even at very high stress. Meyer (1973) has published similar results for ground blocks, but he also shows results for polished surfaces which indicate that the reflection coefficient may approach zero for very smooth surfaces under load. However it is unlikely that real defects are ever sufficiently smooth for this to happen; for instance the fatigue crack studied here had at the start of the growth a roughness of 5μm Ra, compared with 0.2μm Ra for the ground blocks. Nevertheless, it would appear that surface roughness appreciably affects the rate at which transmission and reflection vary with the stress applied. One application of these results is that of testing the tightness of shrunk-on components by measuring the transmission or reflection coefficients. This can only be done accurately if the surface roughness is well controlled so that calibration tests may be performed.

Whereas the measurements on the ground blocks were at normal incidence, those on the fatigue crack used angled beams. If the fatigue cracks were perfectly smooth, there would be no echo from the crack face and indeed, we found that very high sensitivity was required to detect an echo from the smoothest part of the crack where the roughness was only 5μm Ra. Nearer the crack tip, because the change in stress intensity factor increased to as much as 70 $MNm^{-3/2}$ before the loading amplitude was reduced, the crack surface was considerably rougher (13μm Ra). In fact, the part of the crack close to the tip is more akin to a low-cycle fatigue crack because in this region the crack grew at an average rate of 1 mm per 1000 cycles.

The echo recorded from the roughest part of the crack face arises from diffuse scattering of the incident beam by the rough surface. In particular, the small, transverse cracks which were revealed on destructive examination and shown in Fig. 10(b) are likely to reflect sound back to the probe. Since these transverse cracks are most pronounced at the roughest region of the crack, it is difficult to distinguish the effect of isolated transverse cracks from the more distributed roughness of the surface. It is interesting that the echoes from the crack tip and the crack face are similar in magnitude since, whereas the simplest model of the crack tip predicts that the scattering will be in the form of cylindrical waves, that from the face is thought to arise from spherical waves scattered from small areas of surface. Because of the residual stresses which are set up in the steel around the crack tip during fatigue, the scattering from the crack tip is very complicated. Nevertheless, we can speculate that both the tip and the face echo are caused by the combined effect of the small transverse cracks and the asperities on the surface. The echoes from the crack tip exhibited a variable dependence on the load, depending on the type of probe and its exact position (see Figs. 30, a, b and c) and the crack face response was similar. The small transverse cracks are unlikely to be compressed by the application of a stress normal to the main crack, even though the main surfaces of the crack become tight. This may explain why in some cases, the crack echo did not decrease with load as shown in Fig. 30(b). In contrast, the transmission measurements tell us much more about the fraction of the main crack surface which is in contact, and they show a steady increase with load, except for a small fluctuation at low loads which has been explained in terms of the redistribution of stress along the surface of the crack as it closes.

Since it was very difficult to obtain any echoes from the smoother part of the crack, it appears that fatigue cracks grown with a Δk of less than 25 $MNm^{-3/2}$ are too smooth to scatter angled beams diffusely. Detection of such cracks must therefore be based on specular reflection and could be achieved with a tandem technique or using a corner echo should the crack break the surface. Rougher cracks may be detected directly in pulse-echo if the sensitivity is high, since they have responses in the region of 1 mm equivalent flat-bottomed hole size. When compressed, the detectability of the crack was usually reduced, but the maximum reduction was only 12dB. Hence to be sure of detecting the crack even when compressed the sensitivity would need to be further increased by this amount, but this is the worst case observed in these experiments, and the average reduction was much less (about 4dB) as indicated in Fig. 31.

Because of the plastic deformation which occurs during fatigue crack growth, the crack surfaces are not mirror images and are unlikely to mate perfectly (Elber, 1970). Although no measurements were made at normal incidence to the crack, since the roughness is considerably greater than that of the ground blocks, the reflection under the same load is likely to be higher. Consequently large fatigue cracks should be detectable at normal incidence even if they are tightly compressed, but the reflection coefficient may be as low as 0.25, and the sensitivity should be increased to compensate for this.

Welding often induces stresses in metals, and residual stress levels in welds which have been properly heat-treated are typically 60 MNm^{-2} (Heaton, 1973) and may be compressive in some areas. Our results imply that such stresses would reduce defect echoes by between 4 and 8dB depending on the frequency and whether shear or compression waves were used. A drop in reflectivity of 6dB would double the area of the smallest detectable defect. Compressive stresses of 60 MNm^{-2} are likely to make obscuration techniques complete ineffective. For example, a compressed crack could easily have a transmission coefficient exceeding 0.5. Consequently, the obscuration of the beam would be less than 6dB and this could be comparable with the variation in coupling on a non-ideal surface. It is also very difficult to distinguish a continuous crack from a number of unconnected but closely-spaced defects using transmission techniques.

It is difficult to generalise about the effect of compressive stress on the sizing of defects. In some situations, particularly when defects are large, the defect edges may be detectable even when compressed. Consequently, sizing methods which rely on measuring the separation of opposite edges of defects should not be impaired. By contrast, with smaller defects where amplitude sizing techniques have to be used, they may typically be in error by 6 to 12 dB, and consequently the area could be underestimated by a factor of 2 to 4.

5. CONCLUSIONS

1. The reflection of shear or compression waves at normal incidence from an artificial steel-steel interface may be reduced by 4 to 8 dB when an external stress of 60 MNm^{-2} is applied. At still larger stresses the amplitude of the reflected signal decreases further, but more slowly. Changes of similar magnitude occurred in the reflectivity of angled shear wave beams from the fatigue crack, although the variation in reflectivity was not usually monotonic.

   In many cases, the ability of the pulse-echo technique to detect defects should not be seriously impaired if the sensitivity of the test is increased to allow for the reduced response of cracks under static compressive loading. However, because of the changes in reflectivity which may occur at relatively modest stresses, techniques using echo amplitude for sizing will suffer from an additional uncertainty whenever compressive stresses are likely to occur.

2. In the case of 2MHz compression waves, the amplitude of the signal transmitted across the interface between two steel blocks is negligible at zero load but increases to about 90% under a compressive stress of 230 MNm^{-2}. The transmission amplitude of 2MHz 45° shear waves across the fatigue crack was 63% of that transmitted through an uncracked part of the block at a stress of 88MN^{-2}. In any situation where a compressive loading exceeding 15 MNm^{-2} can occur, the accuracy of ultrasonic transmission tests will be severely degraded.

3. The equivalent flat-bottomed hole size of the tip of the fatigue crack studied in this report is small, of the order of 1.0mm, and is substantially independent of the angle of incidence.

4. The magnitude of the diffuse scattering from the face of a fatigue crack depends critically on the crack growth conditions. When the applied stresses are such that the crack growth rate is rapid (Δk greater than 70 MNm^{-2} for BS15 steel) the diffuse scattering from the crack face may produce an echo which is comparable with that from the crack tip.

6. RECOMMENDATIONS

1. When specifying threshold recording levels for automatic in-service ultrasonic inspections or the amplitude at which defect echoes are considered significant during manual inspections, one should allow for the effects of possible compressive stresses. The signal reflected from a crack which is under compression during the test is likely to be reduced by between 6dB and 12dB depending on the crack roughness and the magnitude of the applied stress.

2. When testing critical components, one should consider altering the external loading conditions so as to reduce the compressive stresses in the region being inspected. For example, rotation of a rotor shaft may be possible, so that the static loading exerts a tensile stress on the part being inspected.

3. Further experiments should be carried out on fatigue cracks to investigate the size of corner echoes from compressed surface-breaking cracks, and the ability of tandem techniques to detect compressed embedded cracks. The effect of crack roughness should also be investigated.

7. ACKNOWLEDGEMENTS

The author wishes to acknowledge helpful discussions with a number of colleagues, in particular Dr. J.M. Coffey. Thanks are also due to Mr. W. Laidler for advice on the growth of fatigue cracks, and Mr. L. Fletcher-Boden and Mr. D. Hanstock for practical assistance.

8. REFERENCES

1. Chang, F.H.S. Couchman, J.C., Yee, B.G.W., 1973.
The Effects of stress on the detection of fatigue cracks by ultrasonic techniques.
Proc. 9th Symp. on NDE. San Antonio, April, 1973, 424-433.

2. Coffey, J.M., 1978.
Quantitative Assessment of the reliability of ultrasonics for detecting and measuring defects in thick-section welds.
Proc. Conf. on "Tolerance of Flaws in Pressurised Components",
Inst. Mech. Eng. 16-18 May 1978, London.

3. Collins, R.V. and Black, J.D., 1978.
Field testing and repair of steel transmission poles.
Welding Journal, May 1978. 32-38.

4. Corbly, D.M., Packman, A.F., Pearson, H.S., 1970.
The Accuracy and precision of ultrasonic shear wave flaw measurements as a function of stress on the flaw.
Materials Evaluation, May 1970, 103-110.

5. Elber, W., 1970.
Fatigue Crack Closure Under Cyclic Tension.
Eng. Fract. Mechanics Vol. 2. 1970. 37-45.

6. Elber, W., 1971.
The Significance of Fatigue Crack Closure.
Damage Tolerance in Aircraft Structures ASTM STP 486, 1971, 230-242.

7. Heaton, M.D., 1973.
Policy for Inspection of Fiddler's Ferry CrMoV Pipework, 1974.
C.E.G.B. Report SSD/SN/334/73.

8. Hueter and Bolt, 1966.
Sonics: Techniques for the use of sound and ultrasound in Engineering and Science.
John Wiley Inc. N.Y.

9. Kendall, K., Tabor, D., 1971.
An Ultrasonic Study of the area of contact between stationary and sliding surfaces.
Proc. Roy. Soc. Lond. A. 323. 321-340.

10. Kinsler and Frey, 1967. Fundamentals of Acoustics.
John Wiley and Sons, N.Y.

11. Krautkramer, J. and Krautkramer, H., 1977.
Ultrasonic Testing of Materials. 2nd Ed. p. 29.

12. Lake, Thorp, Barton, Perry, 1975.
Development of stress enhanced ultrasonic compressor blade inspection equipment.
Proc. 10th Symp. on NDE, San Antonio, April 1975.

13. Lidington, B.H., Silk, M.G. et al 1976. Ultrasonic Measurements of the Depth of Fatigue Cracks.
Brit. J. of NDT Nov. 1976.

14. Meyer, H.J., 1973. In-Service Inspection of Reactor Pressure Vessels.
International Symposium on Mechanization and automation of inspection on pressurised plant.
Tokyo, Dec. 19-20. 1973.

15. Serabian, S. and Moriarty, C.D. 1957.
Ultrasonic Detection of thin Laminar inclusions.
ASME Paper 57, PWR 11, 1957.

16. Sziland, J., 1967.
On the ultrasonic detectability of thin slag inclusions in steel plates.
Non-Destructive Testing, Aug. 1967. 45-47.

17. Yee, B.G.W., Couchman, J.C., Hagemeyer, J.W., Chang, F.H., 1974.
Stress and the ultrasonic detection of fatigue cracks in engineering metals.
Non-Destructive Testing, Oct. 1974. 245-250.

18. Yee, B.G.W., Hagemeyer, J.W., 1975.
The effects of relaxation and closure stresses on the detection of fatigue cracks in 2219-T87 Aluminium.
Proc. 10th Symp. on NDE. San Antonio, April 1975.

APPENDIX A

THE CHANGE IN STRESS DISTRIBUTION IN THE PLANE OF THE CRACK AS IT CLOSES

A simplified model for the cracked block has been devised which appears to explain the fluctuations in transmission and reflection from the fatigue crack which were described in Section 3. The block is considered as a homogeneous solid with a saw-cut which progressively closes as the load is applied. It is assumed that, although some plastic deformation may have occurred during crack growth, the stresses set up by compressing the block lie within the elastic limit of the steel. It is further assumed that the stress distribution in the plane of the crack is linear and residual stresses occuring very close to the crack tip have been ignored.

Fig. A1 shows the geometry of the model; the X and Y axes lie in the plane of the crack and distances have been measured from the mid-line of the block along the y-axis. The crack extends to y = b while that part of the crack which is in contact at a given load, L, extends to y = a. The distance between the mid-line of the block and the axis of the applied load is denoted by 'e'.

The width of the block = 2d = 70 mm.

The thickness of the block = w.

σ_y, the stress at a point y, is positive when the stress is tensile.

It is assumed that the stress at a position on the crack is independent of it's position along the x-axis. The starter notch has been excluded from this analysis, but the likely consequences are discussed at the end of this Appendix.

Let us assume that the part of the crack between y = a and y = b is tight, whereas the rest of the crack bears no load.

i.e. $y = o$ for $-d<y<a$

considering the x - y plane and resolving forces,

$$-L = \int_a^d \sigma_y \, dy.w \qquad (1)$$

and taking moments about O, $Le = \int_a^d \sigma_y \, y \, dy. \, w,$ (2)

assuming a linear stress distribution for $y>a$.

Let $\sigma_y = Ky + C$; K and C are constants

Then integrating (1) and (2), we have

$$-\frac{L}{w} = \frac{K}{2}(d^2-a^2) + C(d-a) \qquad (3)$$

and $$\frac{Le}{w} = \frac{K}{3}(d^3-a^3) + \frac{C}{2}(d^2-a^2) \qquad (4)$$

Let $L/W = P$, $d - a = \alpha$, $d^2 - a^2 = \beta$, $d^3 - a^3 = \gamma$,

Then $-P = K/2 \cdot \beta + C\alpha$ (5)

and $Pe = K/3 \cdot \gamma + C/2 \cdot \beta$ (6)

Solving equations 5 and 6 for K and C, we obtain,

$$K = \frac{-P\ (\beta/2 + e\alpha)}{(\beta^2/4 - \frac{\gamma\alpha}{3})}$$

and $$C = \frac{+P(\gamma/3 + e\ \beta/2)}{(\beta^2/4 - \gamma\alpha/3)}$$

Using these values we can calculate the stress σy at point y depending on the amount of the crack surface which is in contact. The results have been plotted in Fig. A2 as the ratio of σy to the mean stress $(\frac{P}{2d})$ for a point at the crack tip (y = 10mm), and a point 20 mm from the tip (y = -10mm). The curves for e = o correspond to uniform loading similar to that achieved in the Denison machine, while those for e = 1 correspond to eccentric loading in the Mand machine.

Considering first the stress near the crack tip, Fig. A2 shows that this is initially highly compressive because there is a large bending moment about this point for low loads. However as more of the crack closes, the ratio $\sigma tip/\sigma mean$ decreases rapidly towards the limiting value of unity attained when the crack is fully closed. The curves for e = o and e = 10 are very similar, indicating that the stress at the tip does not vary much between the two loading conditions, as discussed in Section 3.5.

Fig. A2 also shows the curves for a point on the crack face, 20mm from the tip, the stress ratio exhibits smaller changes than those of the tip because the bending moment is reduced as the crack progressively closes. However the effect of the different loading arrangements is more pronounced than in the case of the crack tip.

The effect of the starter notch has not been included in the model of Fig. A1, but we may approximate it by assuming that the part of the crack for y>26mm never becomes tight. Consequently by referring to Fig. A2 we can see that there is always a small variation in stress across the crack, when e = o or 10, being most compressive close to the starter notch when the crack is fully closed.

In practice, the stress distribution on the crack is likely to be considerably more complicated than predicted by this model. In particular, residual compressive stresses are likely to occur in the steel surrounding the crack tip because of the plastic deformation which occurs during crack growth. Such stresses may cause slight bowing of the crack as it closes. Because of the plastic deformation which occurs at the advancing crack tip, the two surfaces do not mate perfectly (Elber 1970, Elber 1971) and this deformation is greatest where the stress intensity is a maximum. However Yee and Hagemeyer (1975) have shown that the residual stresses around the crack tip may cause slow closure of the crack faces and give rise to a reduction in the ultrasonic response with time, but the effects they recorded were most noticeable with small tight cracks less than about 5mm long.

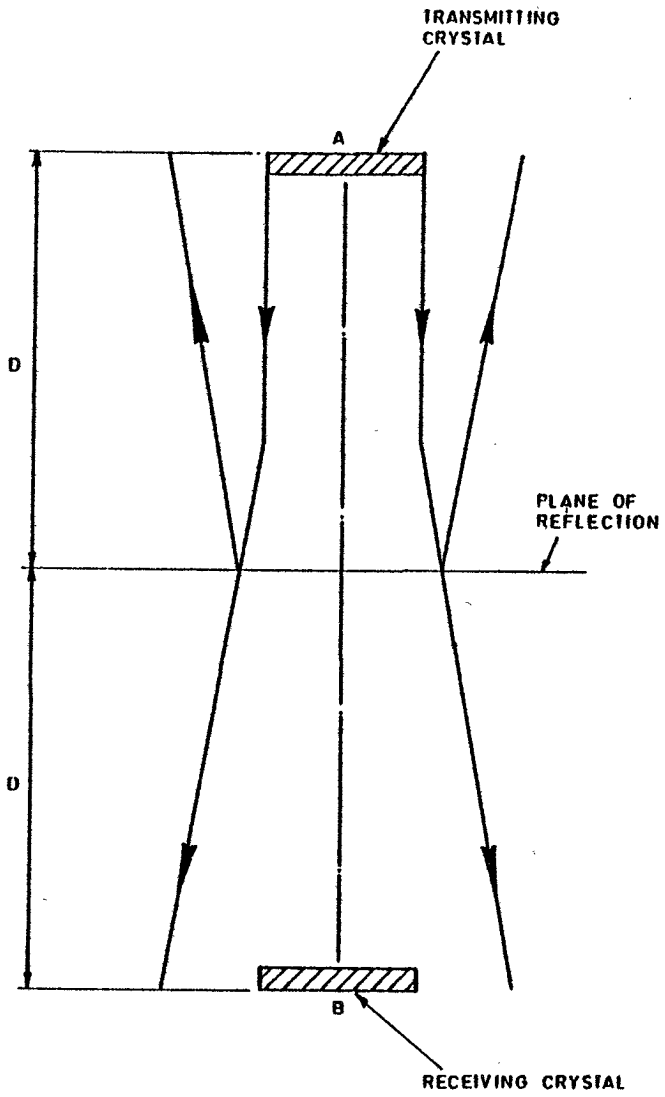

FIG. 2 THE SYMMETRY OF THE TRANSMITTED AND REFLECTED BEAMS

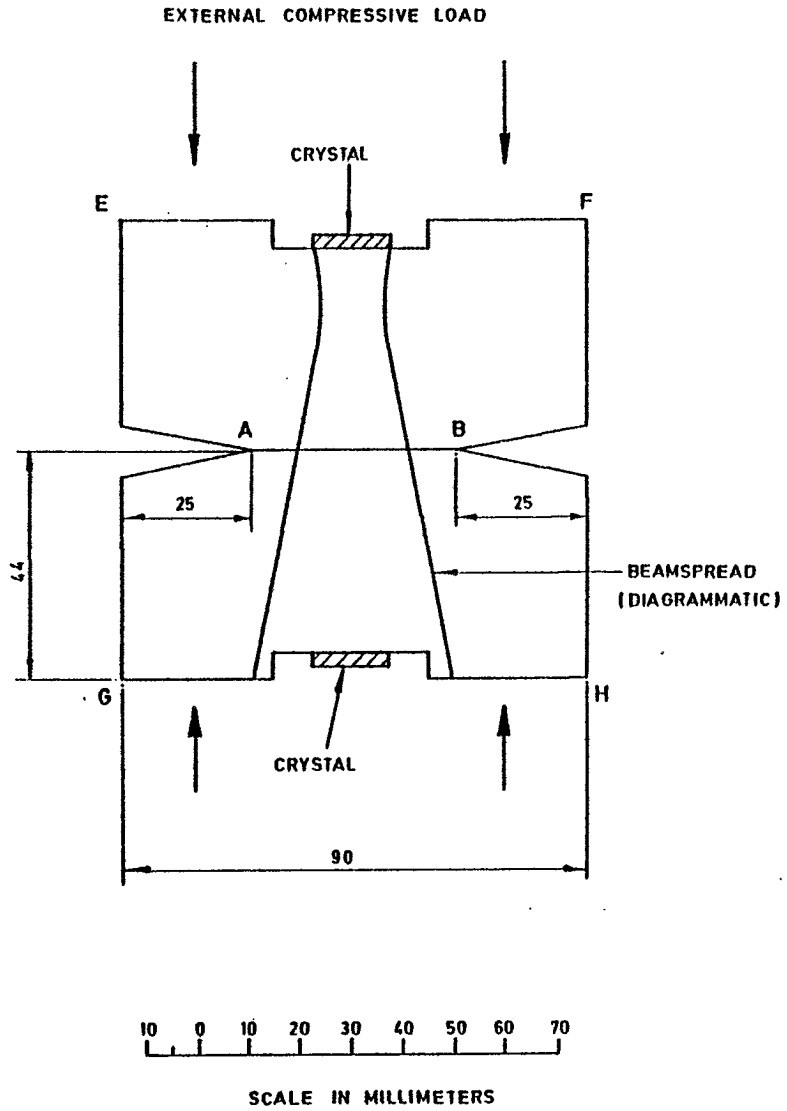

FIG. 1 A VERTICAL SECTION THROUGH THE STEEL BLOCKS

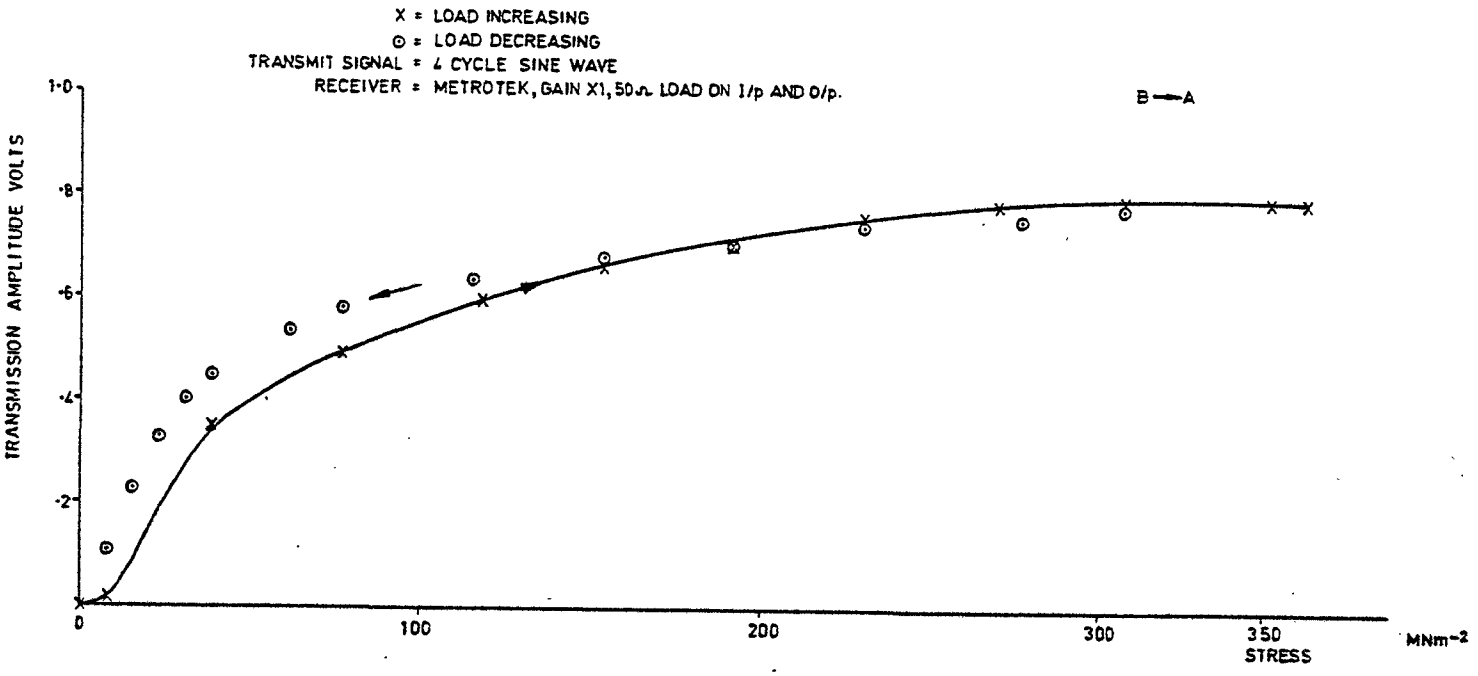

FIG. 3(a). TRANSMISSION VERSUS LOAD FOR 2MHz COMPRESSION WAVES. GROUND STEEL FACES – DRY.

RC/SSR/AL/948

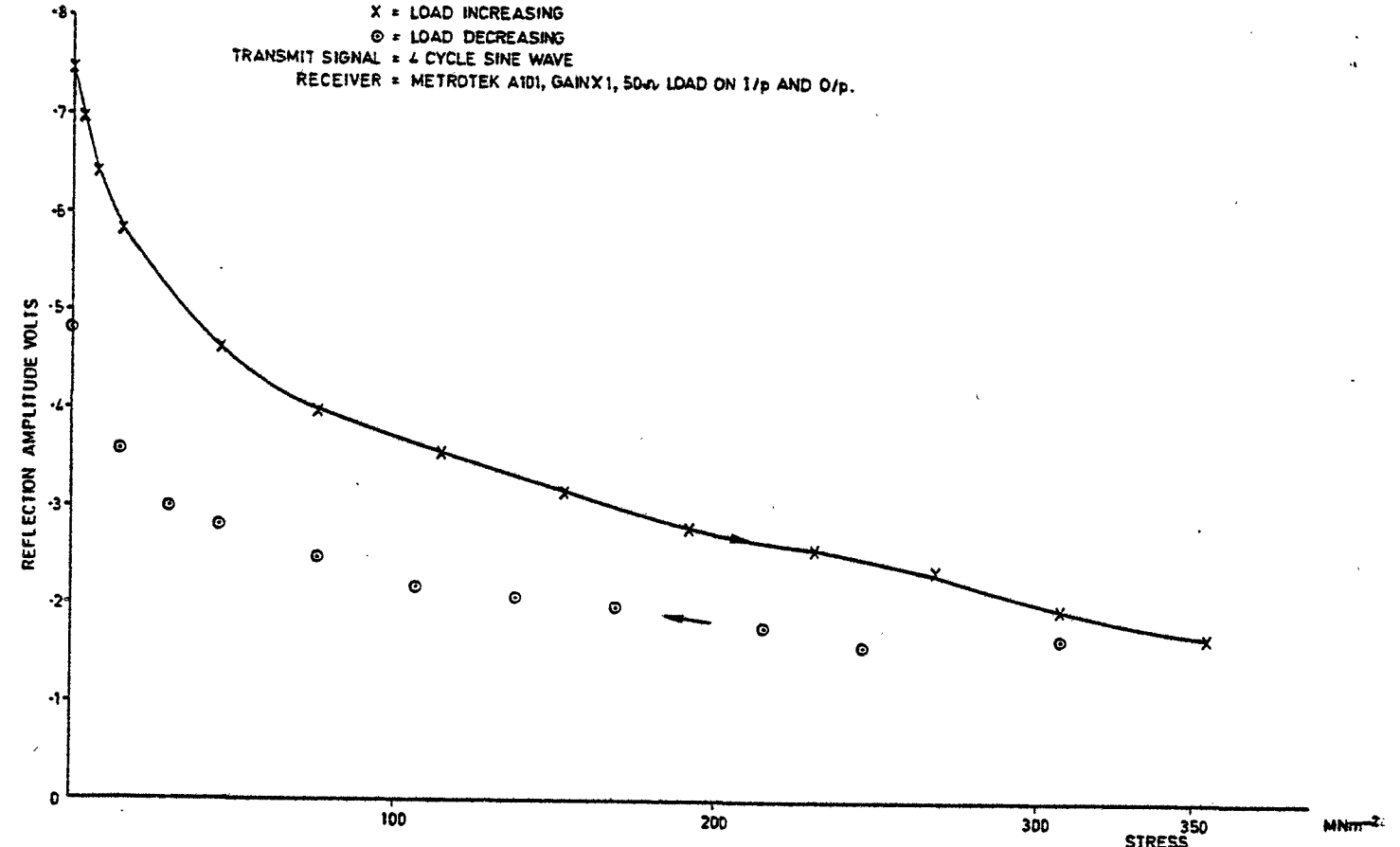

FIG. 3(b). REFLECTION VERSUS LOAD FOR 2MHz COMPRESSION WAVES - GROUND STEEL FACES - DRY.

RC/SSR/AL/958

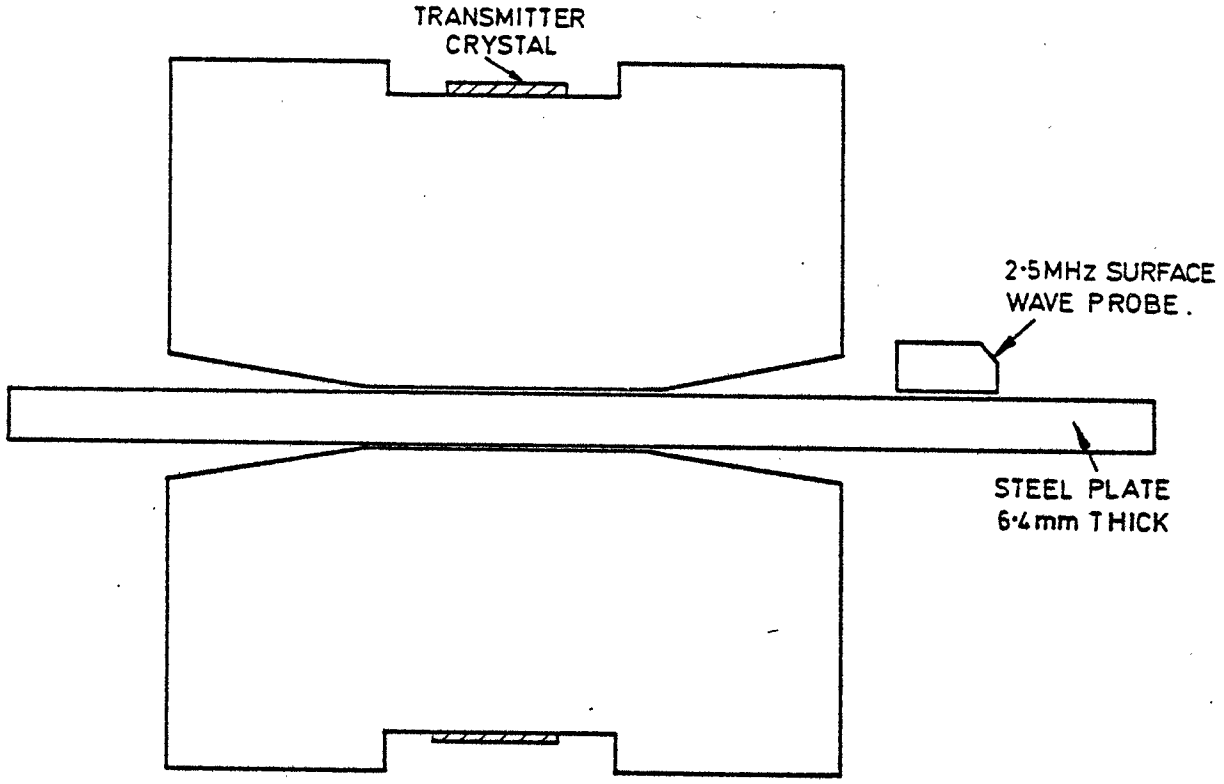

FIG. 5. DETECTION OF SURFACE WAVES PRODUCED AT THE INTERFACE

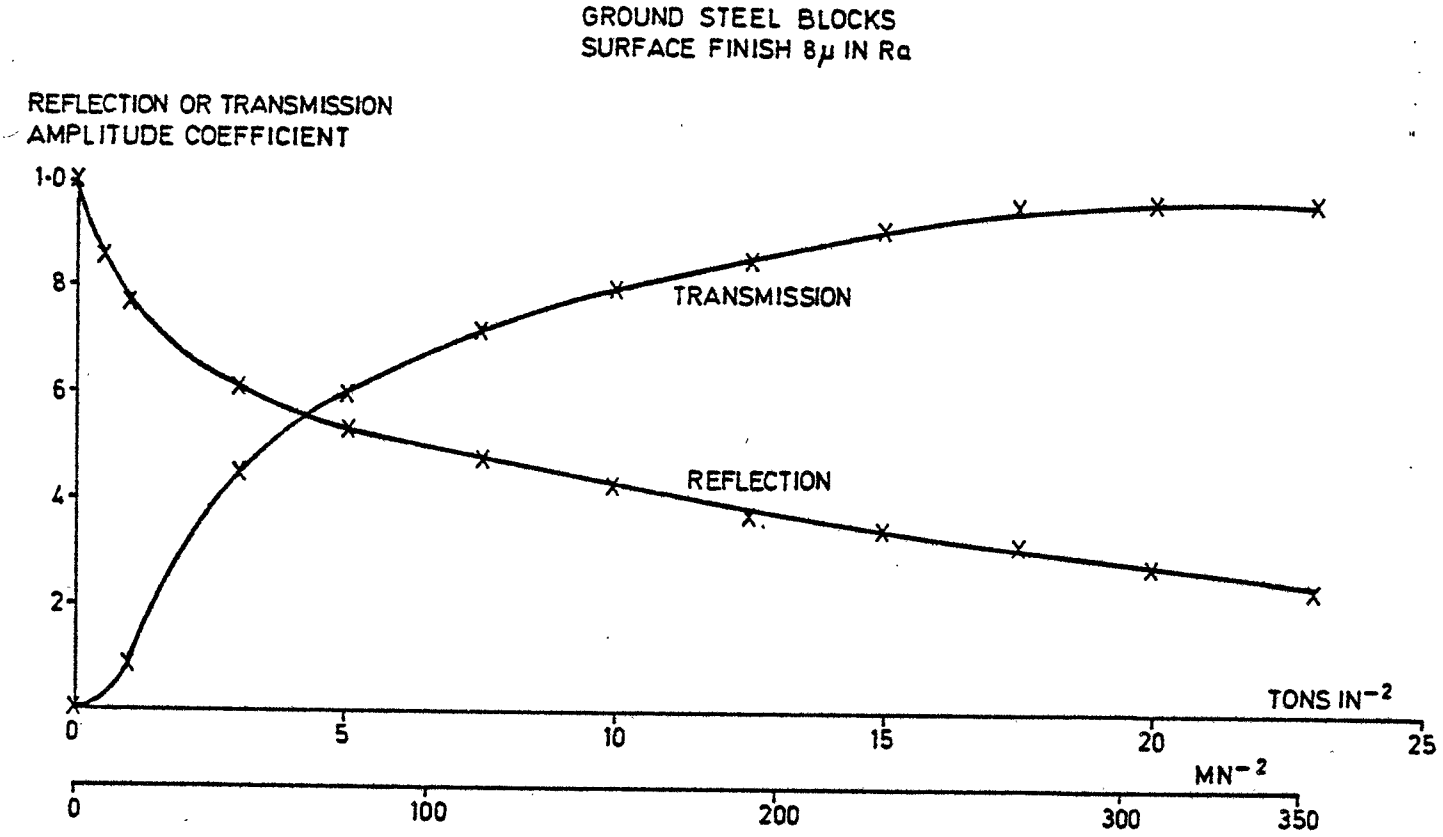

FIG. 4. REFLECTION AND TRANSMISSION COEFFICIENT FOR 2MHz COMPRESSION WAVES.

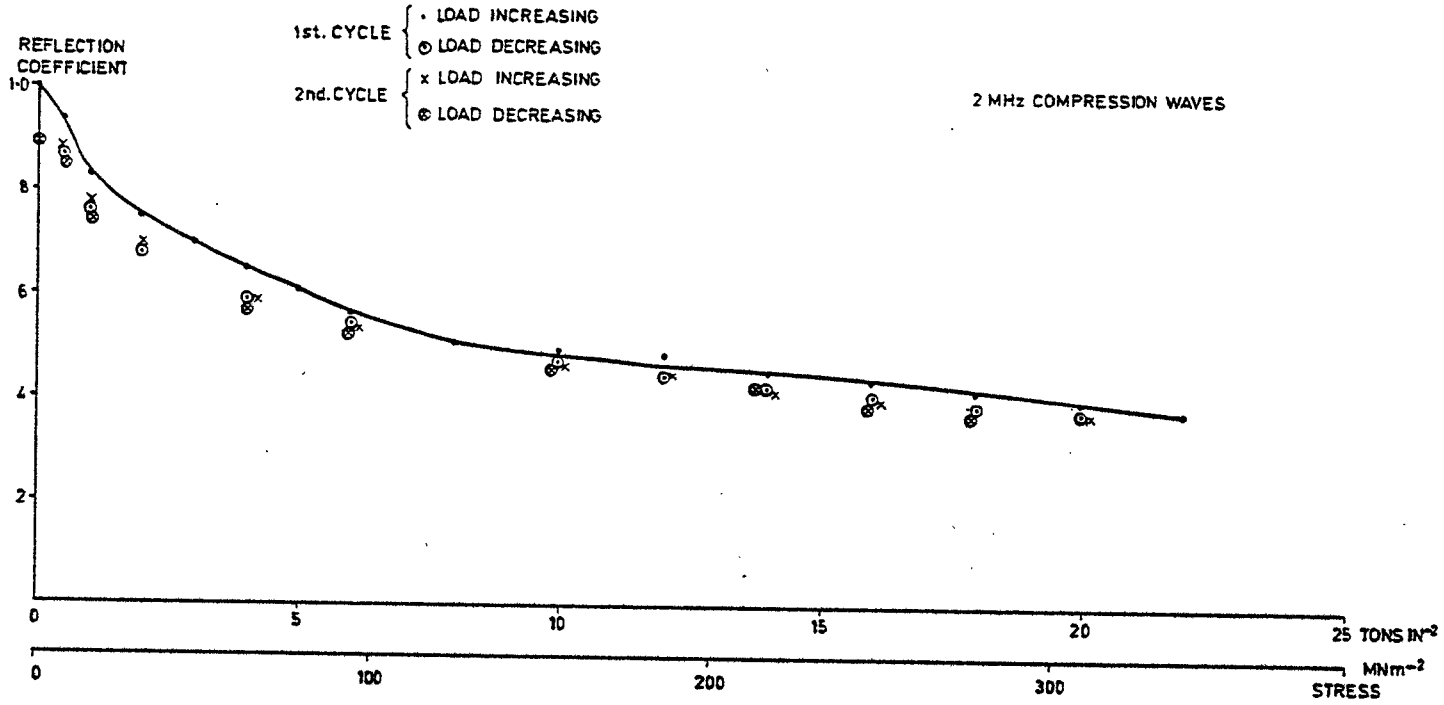

FIG. 6(a). REFLECTION COEFFICIENT FOR TWO COMPLETE LOADING CYCLES. STEEL BLOCKS FREE TO MOVE.

RC/SSR/A4/952

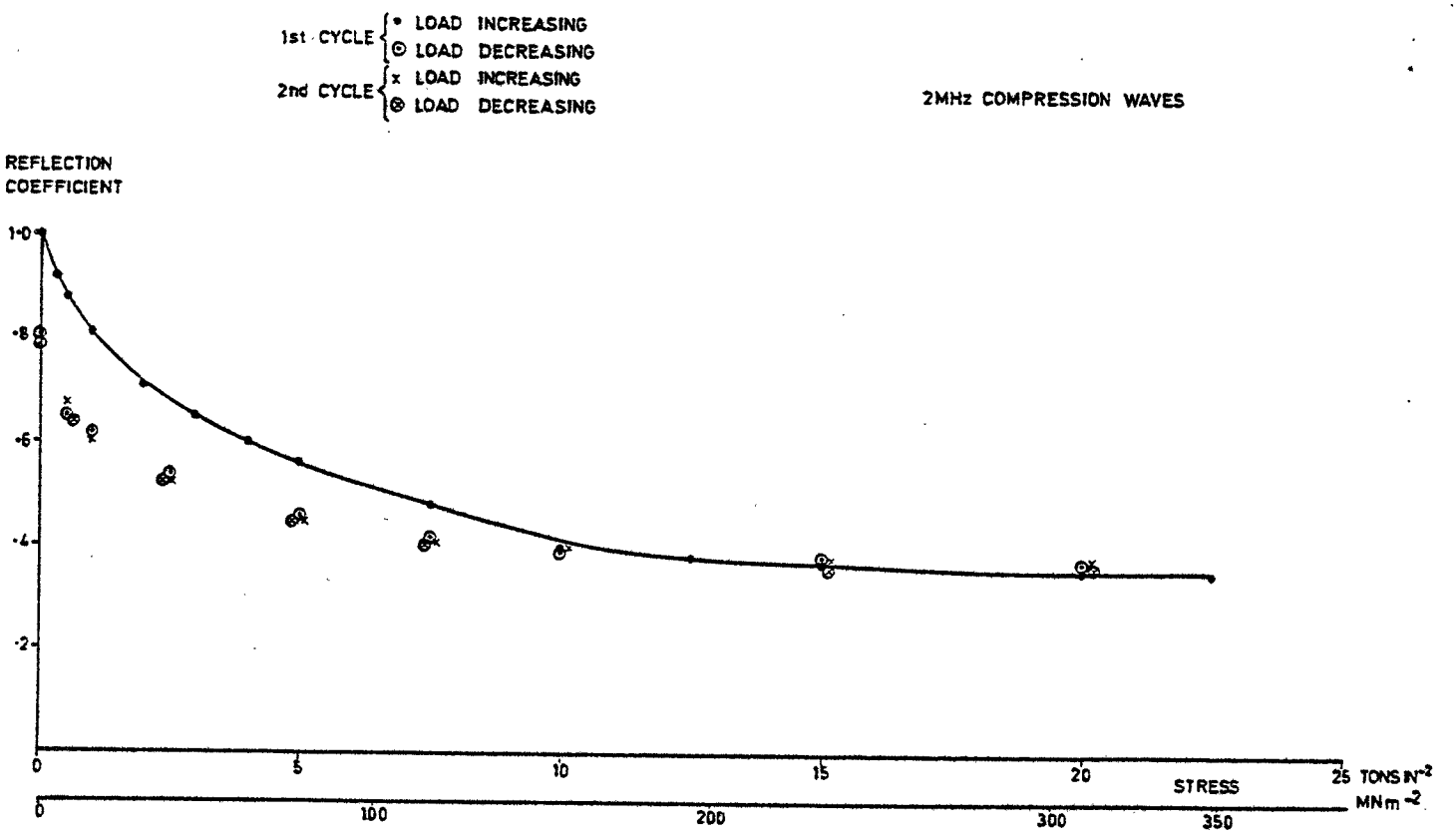

FIG. 6(b). REFLECTION COEFFICIENT FOR TWO COMPLETE LOADING CYCLES. STEEL BLOCKS HELD TOGETHER WITH WELDED PINS.

RC/SSR/A4/953

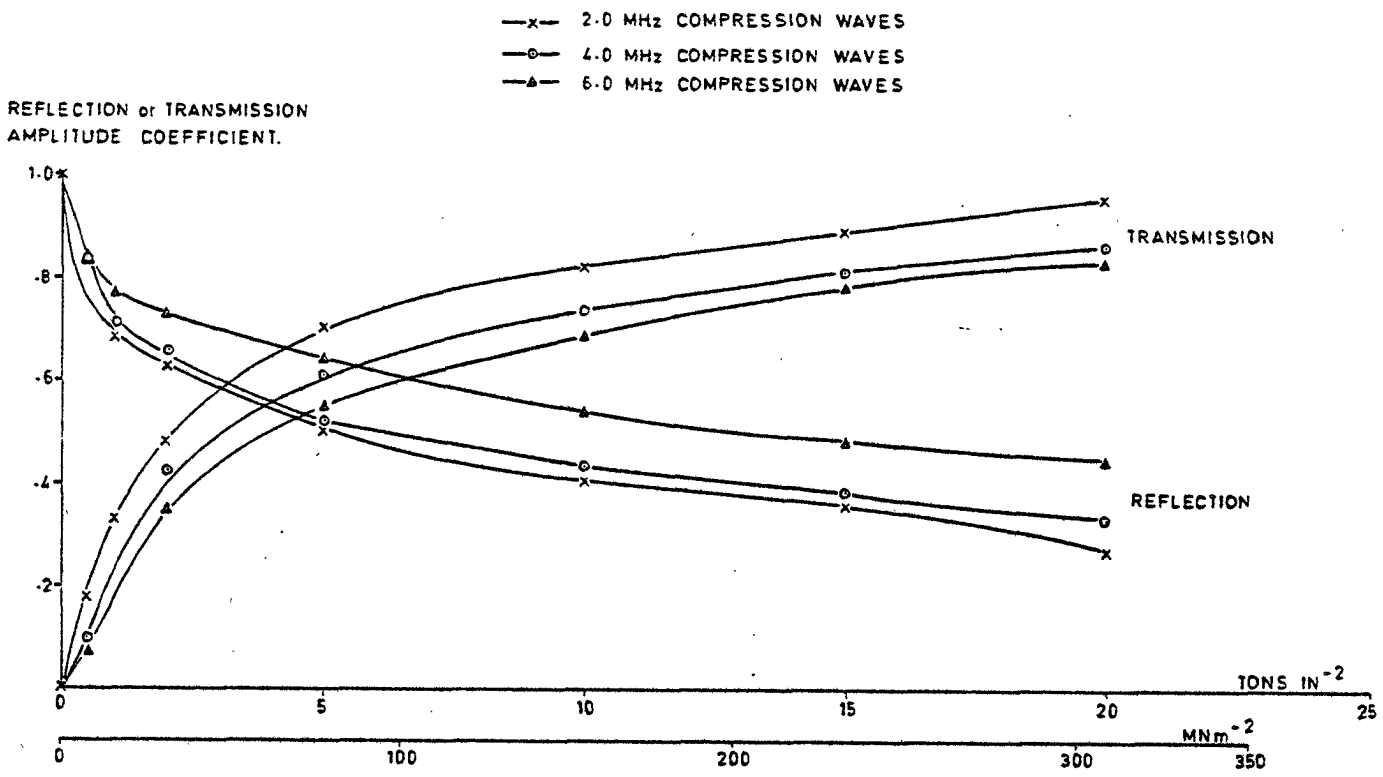

FIG.7 THE FREQUENCY DEPENDENCE OF THE REFLECTION & TRANSMISSION COEFFICIENTS

RC/SSR/A4/849

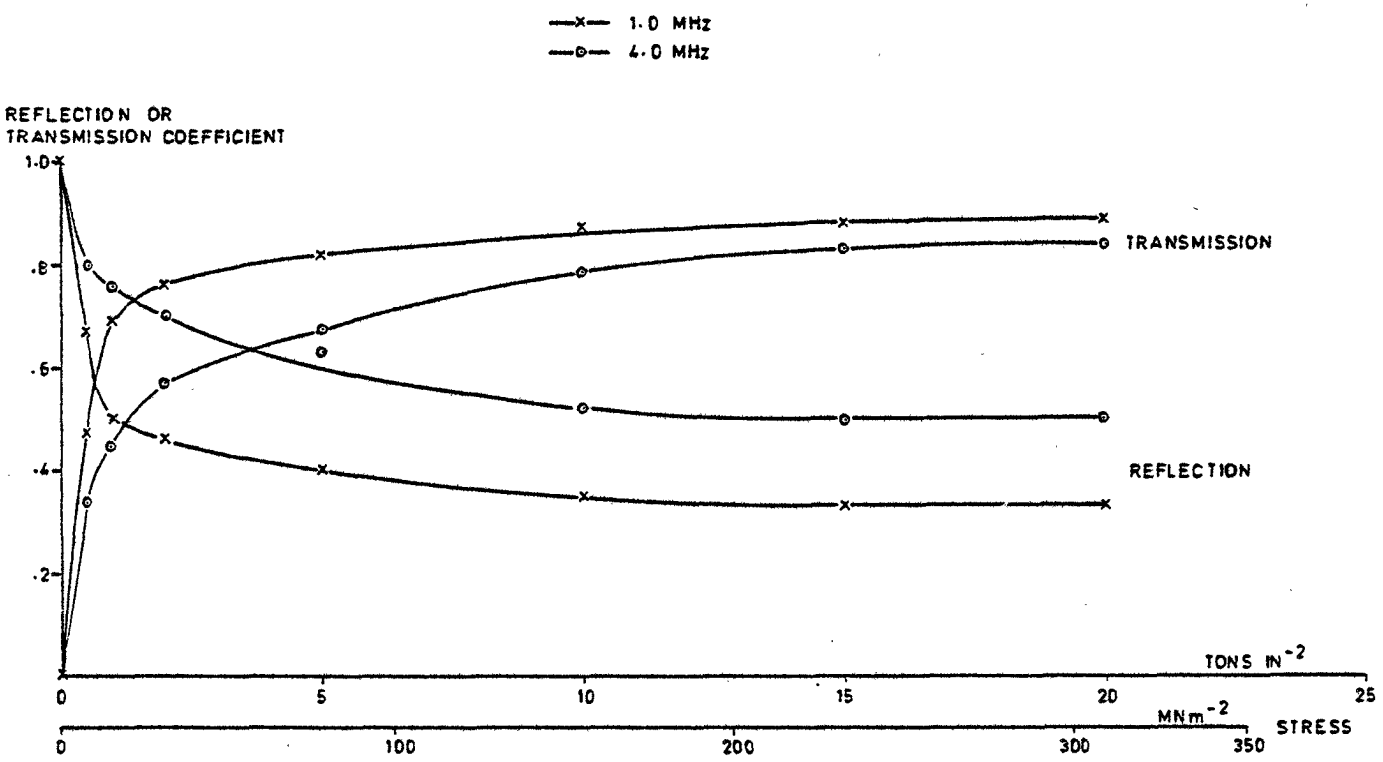

FIG.8 REFLECTION & TRANSMISSION COEFFICIENTS FOR SHEAR WAVES

RC/SSR/A4/850

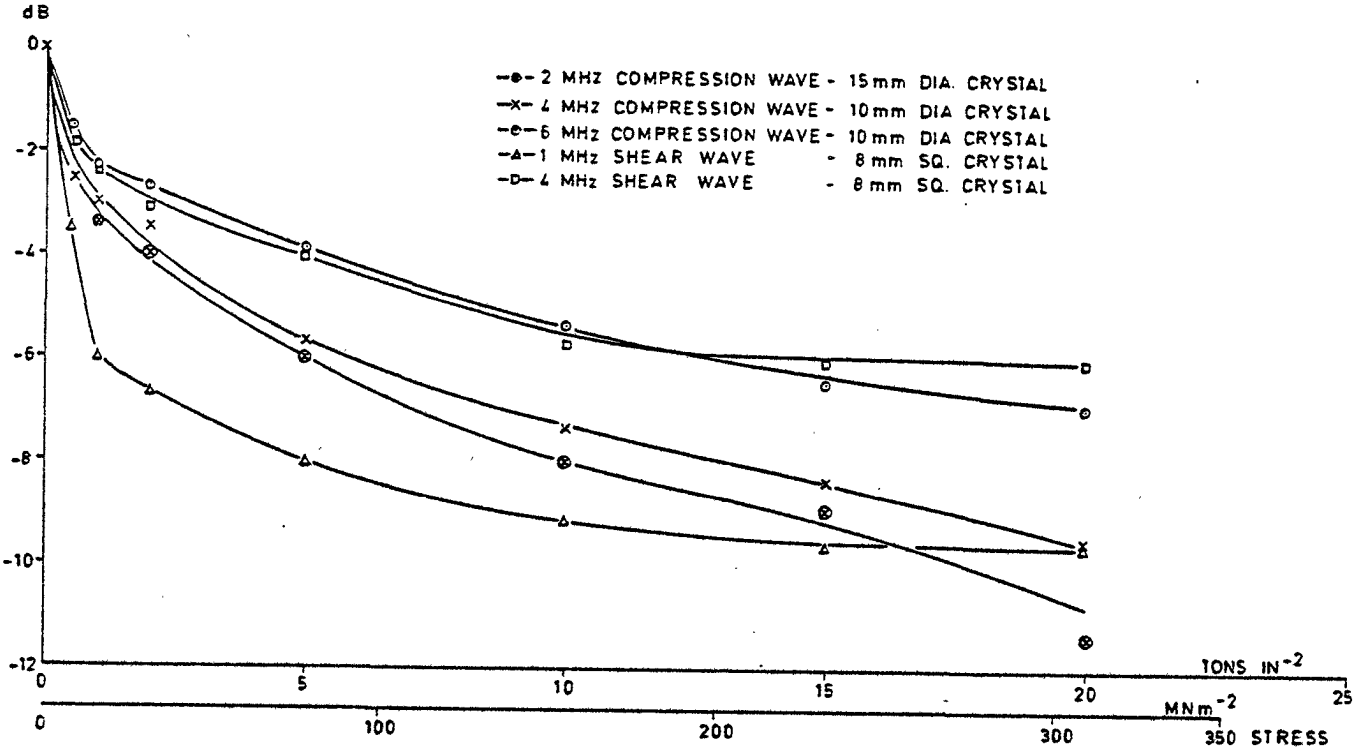

FIG. 9 CHANGES IN REFLECTION WITH APPLIED LOAD (dB SCALE)

RC/SSR/A4/851

4·0 MHz COMPRESSION WAVES
x GROUND STEEL FACES.
⊙ PAD 1 - AREA OF CONTACT (OPTICAL) - 34%
Δ PAD 2 " " " " - 92%
□ PAD 3 " " " " - 95%

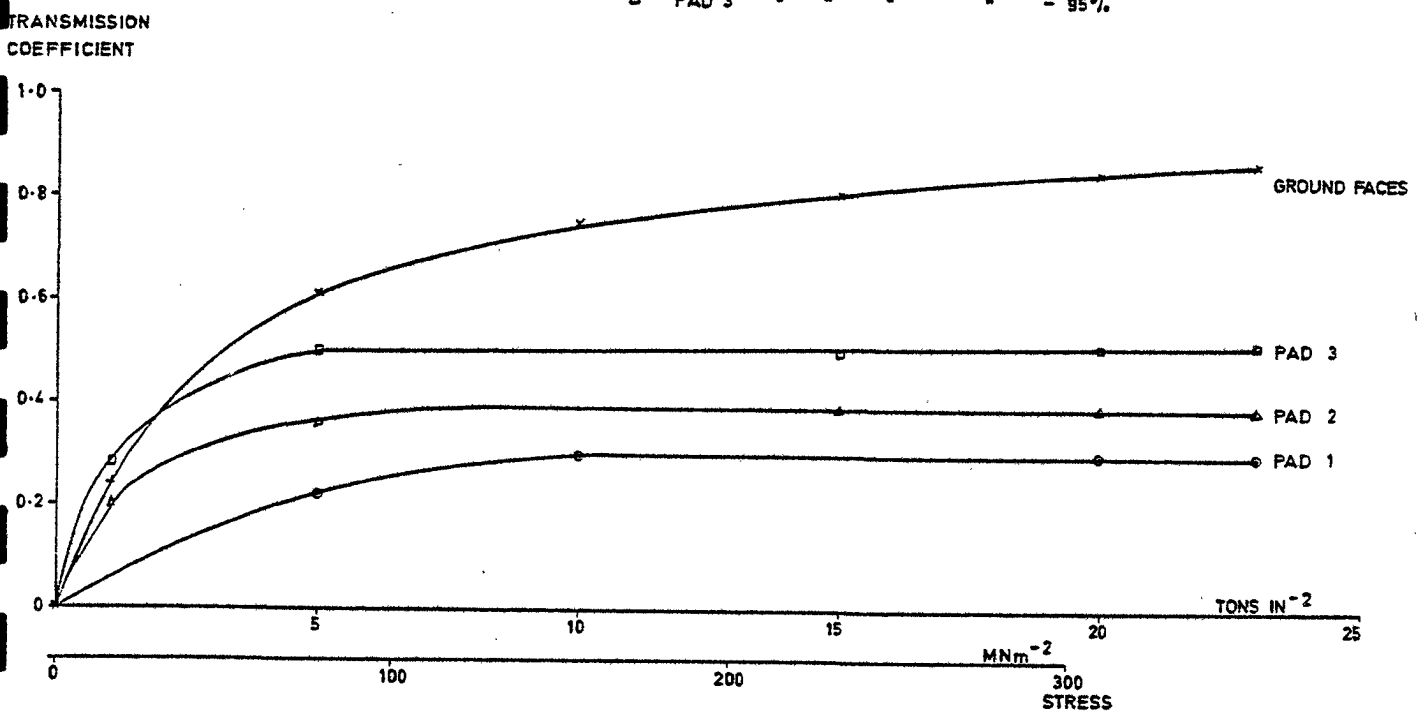

FIG. 10 TRANSMISSION THROUGH STEEL WOOL PADS OF VARYING THICKNESS

RC/SSR/A4/853

	THICKNESS	AREA OF CONTACT AC	AMPLITUDE TRANSMISSION COEFFICIENT AT 350 MNm^{-2}	TRANSMISSION / $\sqrt{AC}$
PAD 1	75 μm	34%	·37	·60
PAD 2	125 μm	92%	·42	·44
PAD 3	200 μm	95%	·52	·53

FIG. 11. THE TRANSMISSION COEFFICIENT FOR THREE STEEL WOOL PADS.

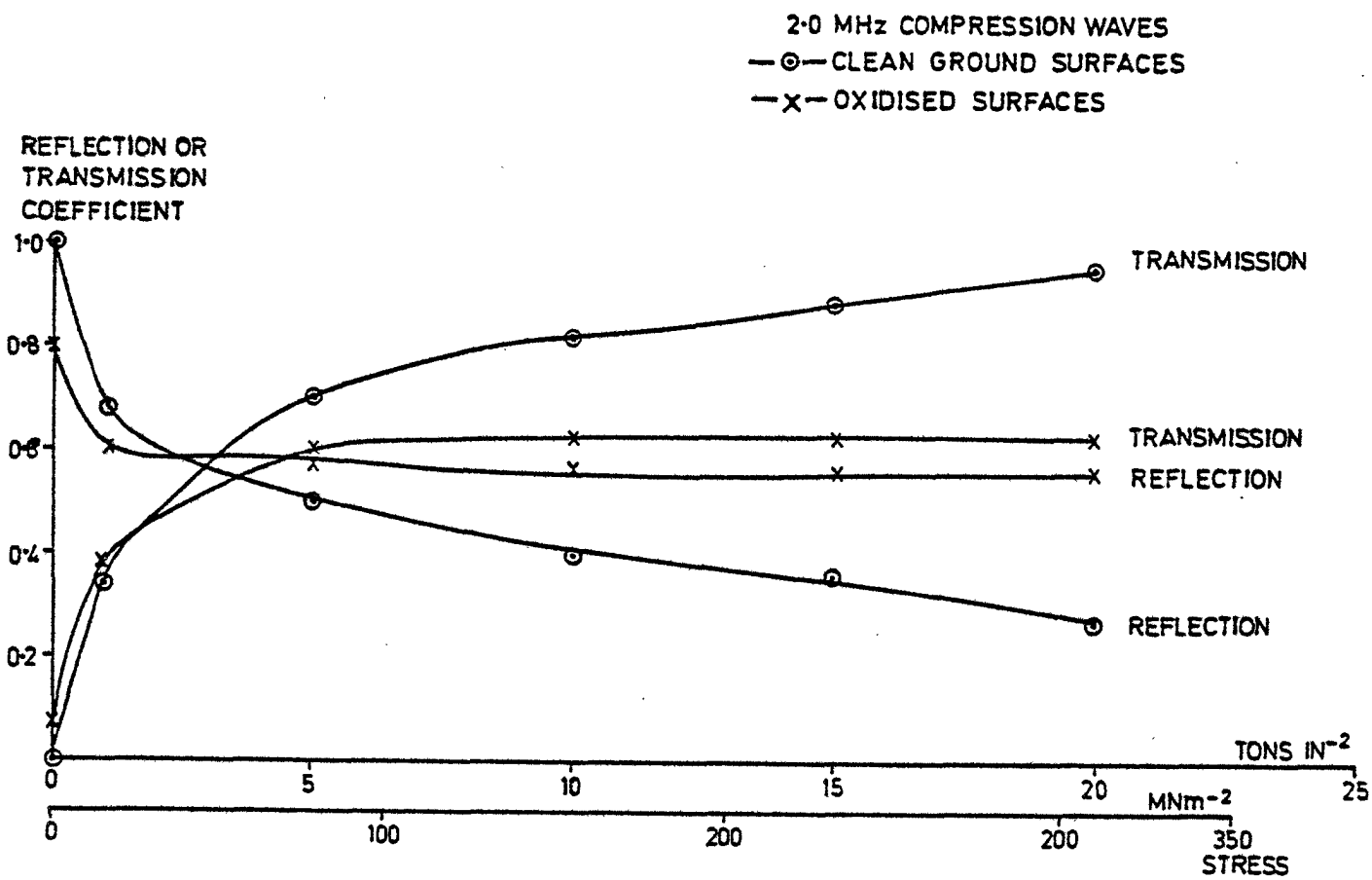

FIG. 12. THE EFFECT OF CORROSION ON TRANSMISSION AND REFLECTION.

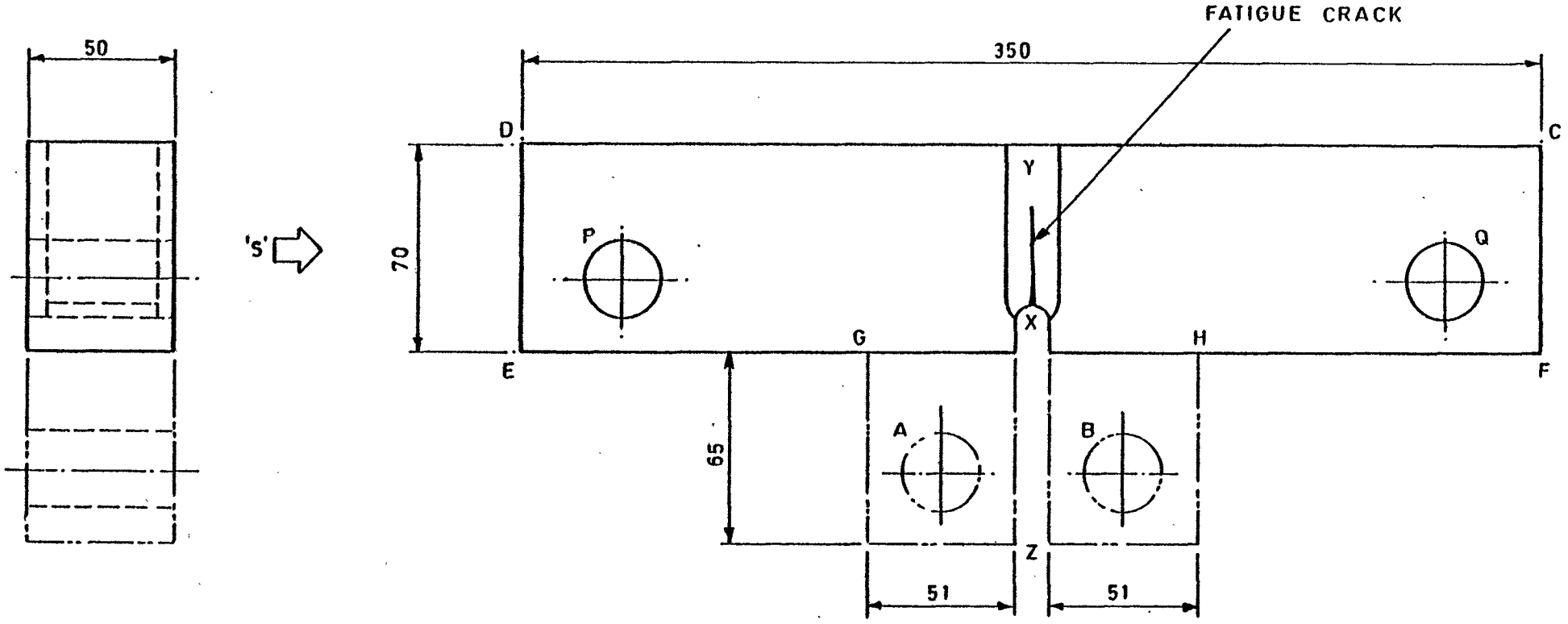

FIG.13 MILD STEEL FATIGUE CRACK SPECIMEN

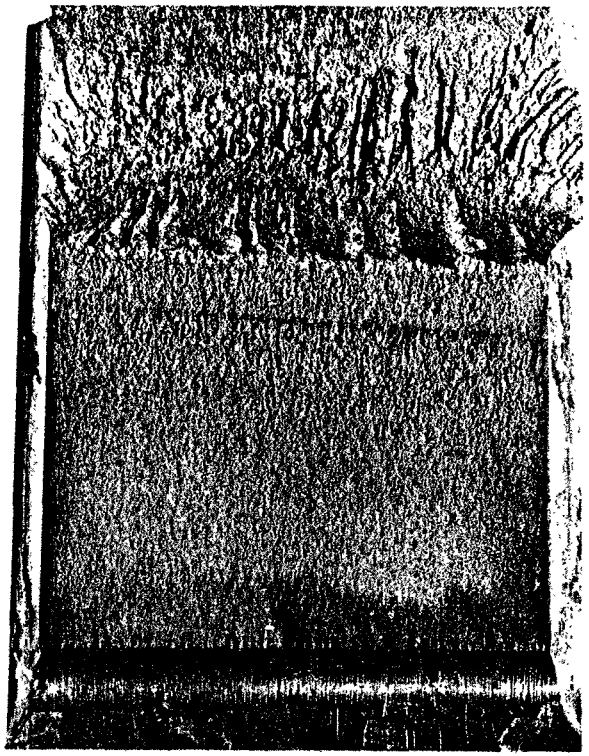

FIG. 14(a) PHOTOGRAPH OF THE FATIGUE CRACK SURFACE.

FIG. 14(b) ELECTRON MICROSCOPE PICTURE TAKEN AT THE REGION OF MAXIMUM ROUGHNESS.

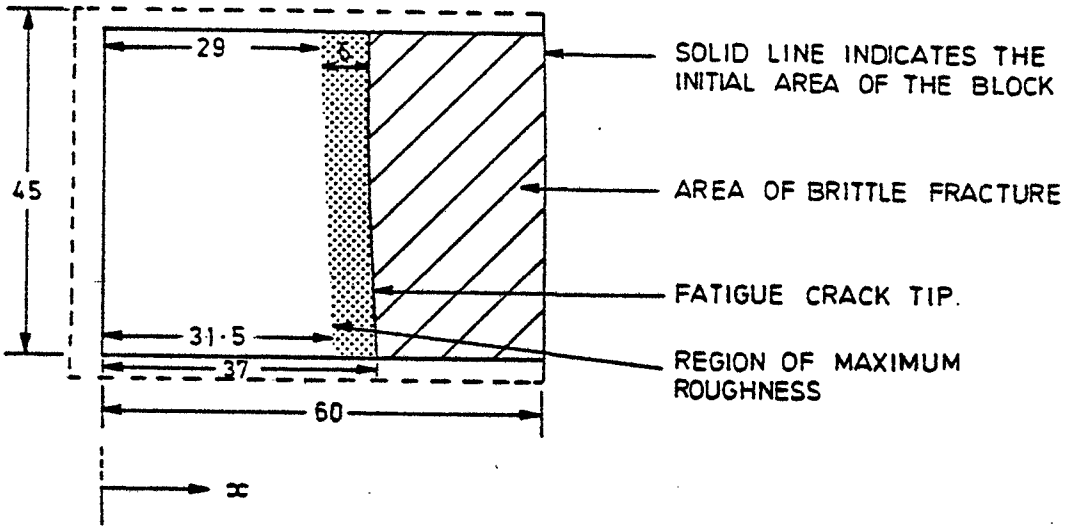

DIMENSIONS SHOWN IN mm .

FIG·15(a). A PLAN VIEW OF THE FATIGUE CRACK.

CRACK LENGTH - x (mm)	PREDICTED GROWTH RATE $(\Delta K)^3$ 10^{-8} m/cycle	ROUGHNESS Ra (μm)	CORRELATION. LENGTH (μm)
0	15·6	7	-
6	22·4	7	0·10
12	36·9	7	0·10
18	73·0	9	0·13
26	195·1	13	0·13
30		17	0·14

FIG·15(b). MEASURED VALUES OF ROUGHNESS AND CORRELATION LENGTH AND PREDICTED VALUES OF THE GROWTH RATE AT VARIOUS POSITIONS ALONG THE CRACK.

FIG 15. THE FATIGUE CRACK SURFACE

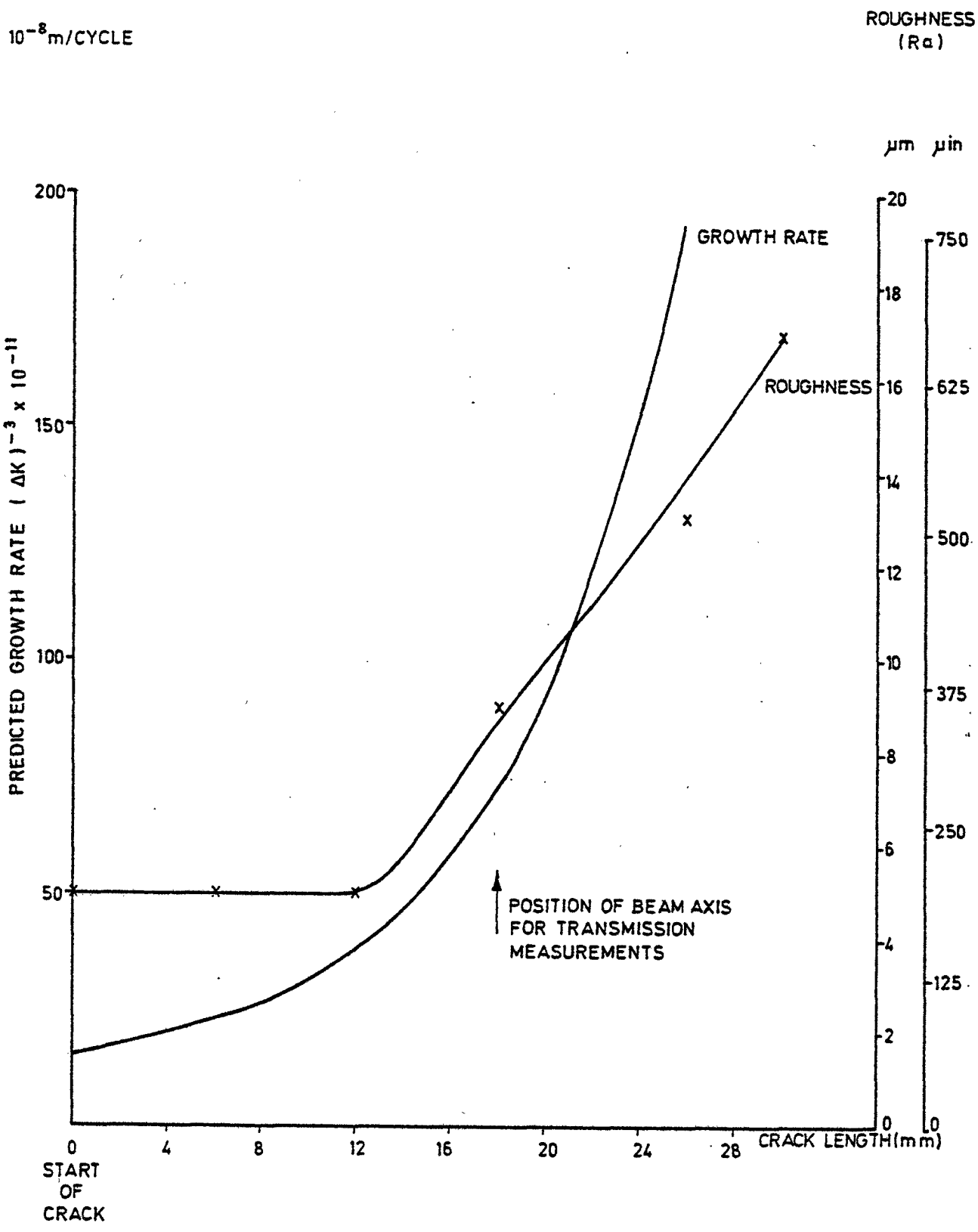

FIG. 16. A COMPARISON OF PREDICTED GROWTH RATE WITH ROUGHNESS ALONG THE CRACK.

PROBE TYPE No.	MAKE	FREQUENCY (MHz)	CRYSTAL DIAMETER (mm)	PROBE SHOE ANGLES °	20 db PULSE LENGTH (μ sec)	NEAR FIELD LENGTH(mm) IN STEEL
1	BAUGH AND WEEDON	5·0	10	45 60 70	1·1	30
2	PANAMETRICS ACCUSCAN	5·0	12·5	45 60 70	1·1	47
3	PANAMETRICS ACCUSCAN	5·0	6·3	45 60 70	1·0	12
4	SONICS	2·25	12·5mm SQUARE (LEAD METANIOBATE)	45 60	1·4	27
5	BAUGH AND WEEDON	2·0	15	45 60 70	3·2	25
6	INSPECTION INSTRUMENTS	2·0	15	NORMAL COMPRESSION	1·6	19

PROBE TYPES 2, 3, AND 4 HAVE INTERCHANGEABLE WEDGES .

FIG.17. ULTRASONIC PROBES USED FOR MEASUREMENTS ON THE FATIGUE CRACK.

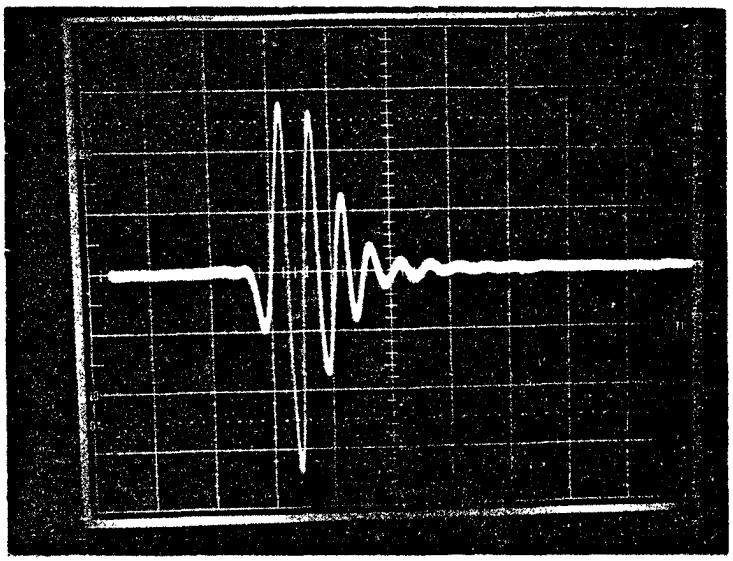

20 db PULSE LENGTH :-1·1μ SEC.
BAUGH AND WEEDON 5MHz 45° 10mm DIA. CRYSTAL.

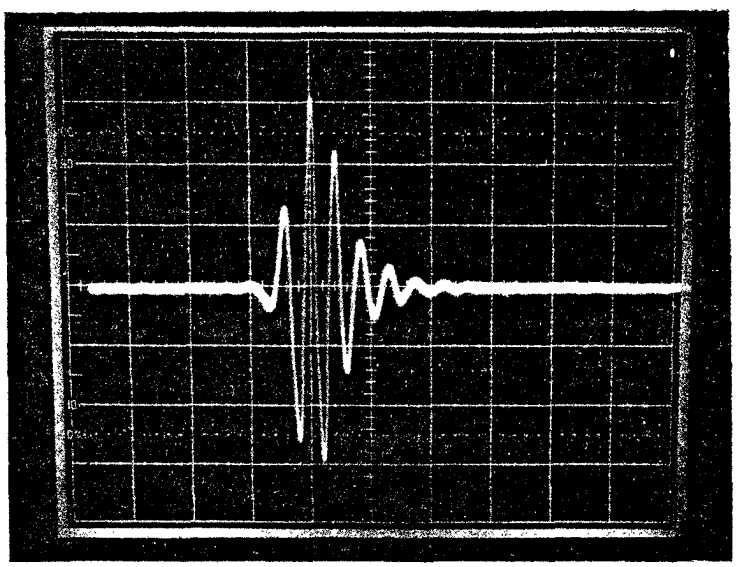

20dB PULSE LENGTH :-1·2μ SEC.
PANAMETRICS 5MHz 60° WEDGE
12·5mm DIA. CRYSTAL.
HORIZONTAL SCALE :- 0·5μ SEC/DIV.
REFLECTOR:- 50mm RADIUS STEEL BLOCK.
METROTEK A101 PULSER-RECEIVER.

FIG.18 TYPICAL ECHOES OBTAINED USING A STANDARD REFLECTOR.

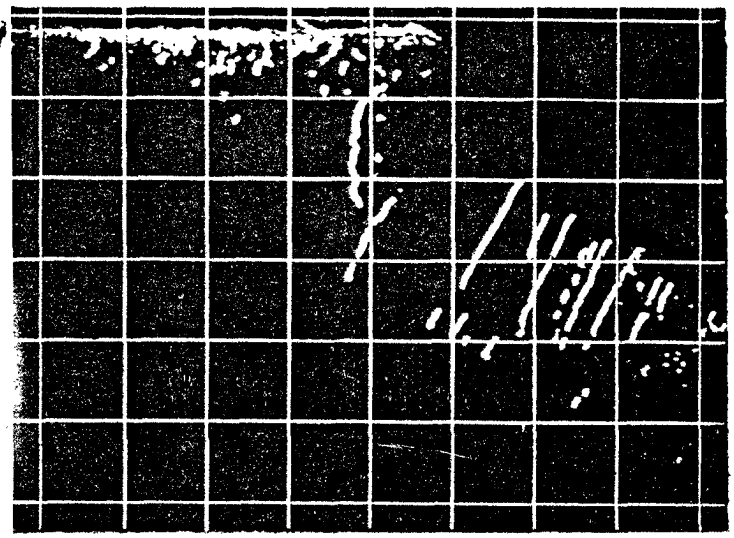

PROBE :- 60° 5 MHz BAUGH AND WEEDON
SCALE :- 1 DIVISION = 20 mm

DISPLAY SENSITIVITY :- 64 dB ABOVE ECHO FROM 50 mm RADIUS.

(a) PHOTOGRAPH

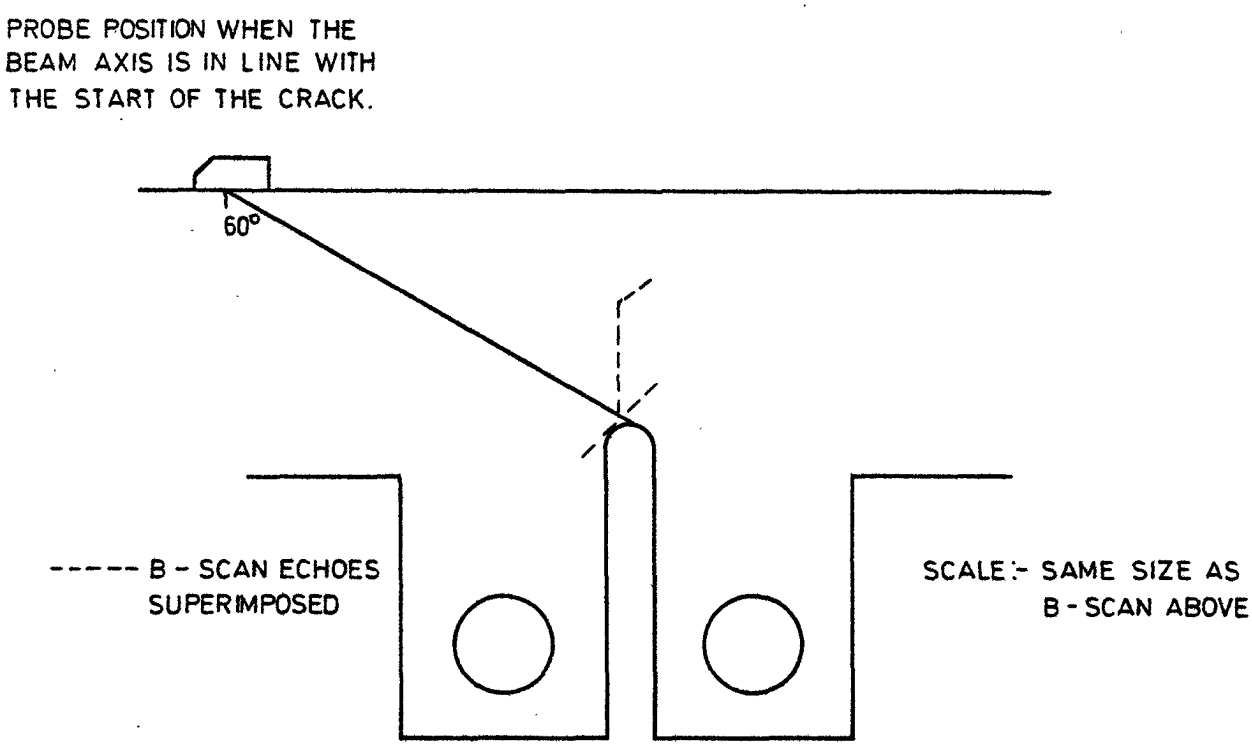

(b) THE BLOCK GEOMETRY

FIG. 19. A 60° B - SCAN OF THE FATIGUE CRACK UNDER NO LOAD.

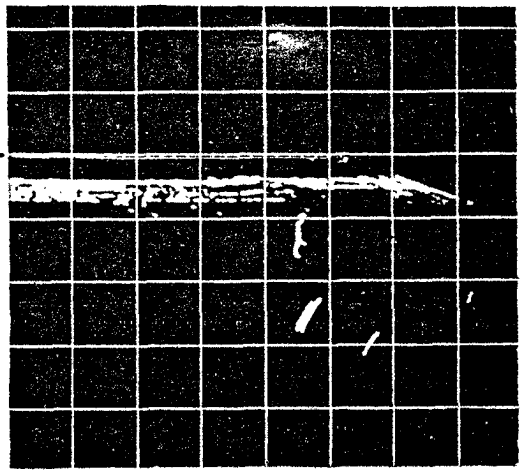

SCALE :- 20mm PER DIVISION.

PROBE:- BAUGH AND WEEDON 5MHz 70°

DISPLAY SENSITIVITY:- 44dB ABOVE ECHO FROM 50mm RADIUS.
ZERO LOAD.

FIG. 20a 70° B-SCAN OF THE CRACK.

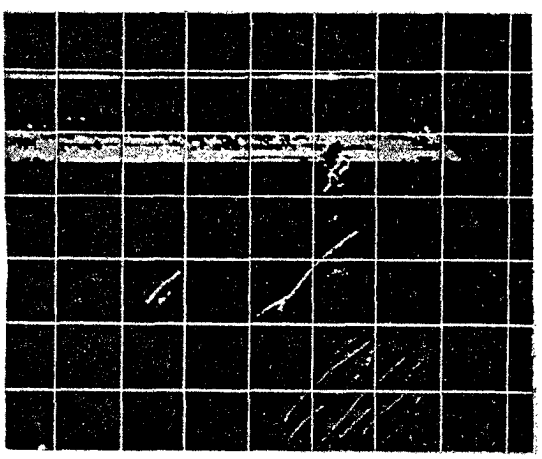

PROBE:- BAUGH AND WEEDON 5MHz 45°

DISPLAY SENSITIVITY:- 52 dB ABOVE ECHO FROM 50mm RADIUS

FIG. 20 b 45° B-SCAN OF THE CRACK.

PROBE:- BAUGH AND WEEDON 5MHz 60°

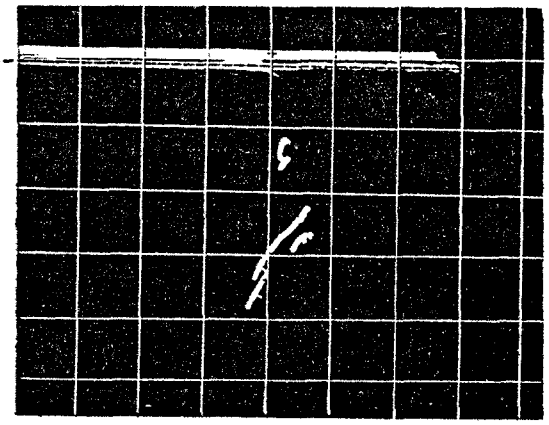

(a) DISPLAY SENSITIVITY:-
46dB ABOVE ECHO
FROM 50mm RADIUS.

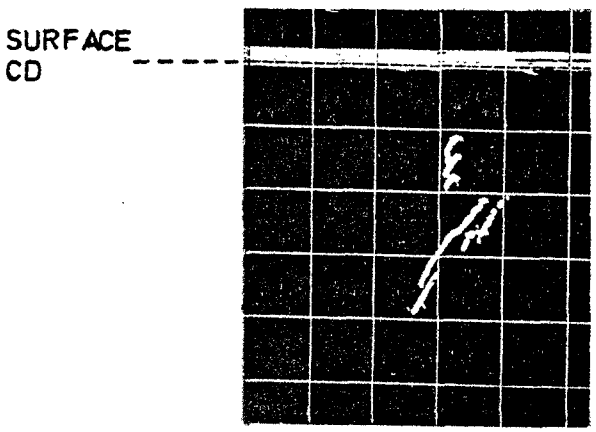

(b) DISPLAY
SENSITIVITY :- 50dB

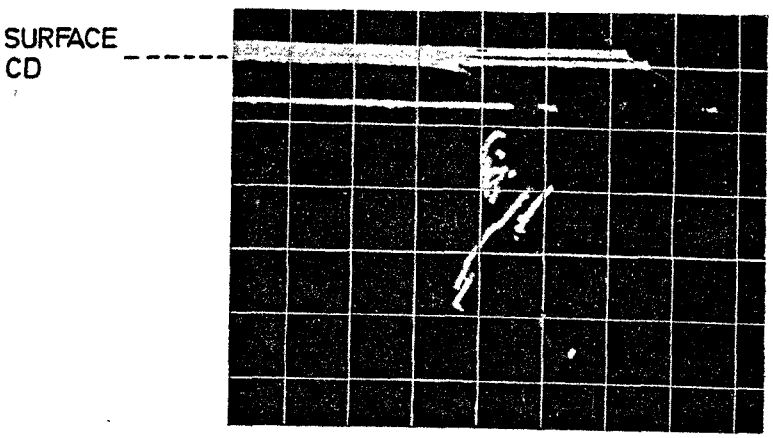

(c) DISPLAY
SENSITIVITY :- 54dB

FIG. 21. 60° B-SCANS AFTER REMOVAL OF THE SIDE ARMS.

A
60° PROBE

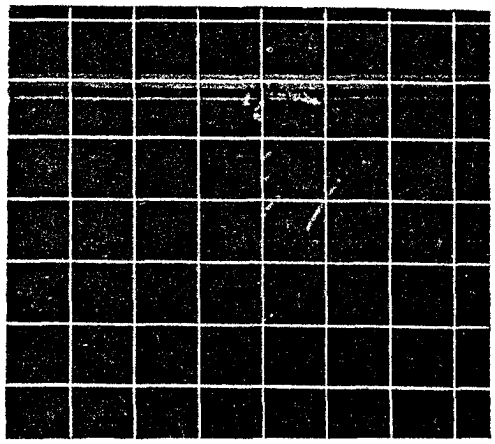

-- SURFACE EF

DISPLAY SENSITIVITY :-
40 dB ABOVE 50mm RADIUS ECHO

B
60° PROBE

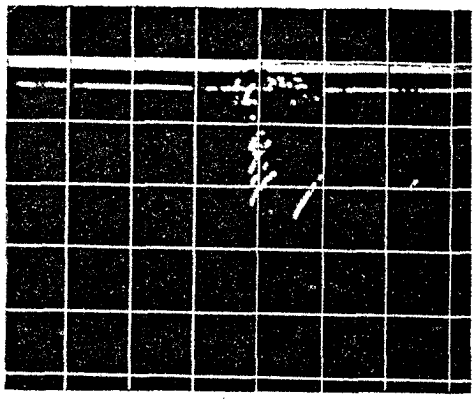

42dB

C
60° PROBE

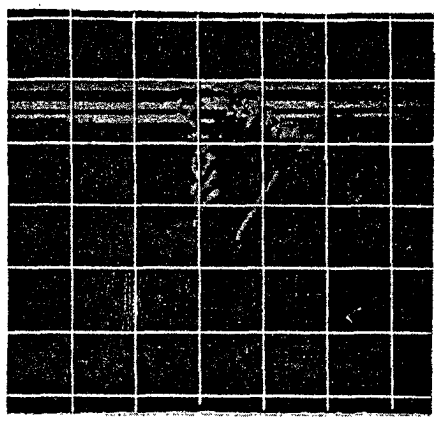

46dB

D
70° PROBE

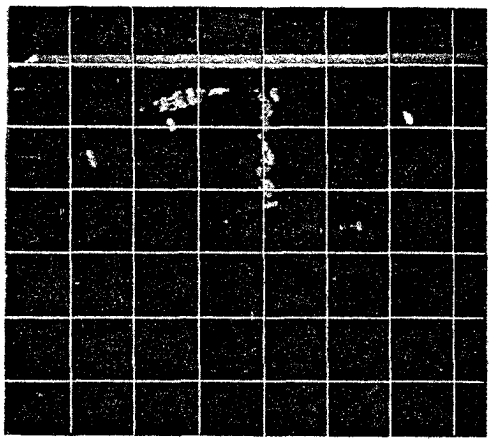

50dB

FIG. 22. B-SCANS OBTAINED FROM THE BOTTOM SURFACE (EF) OF THE BLOCK.

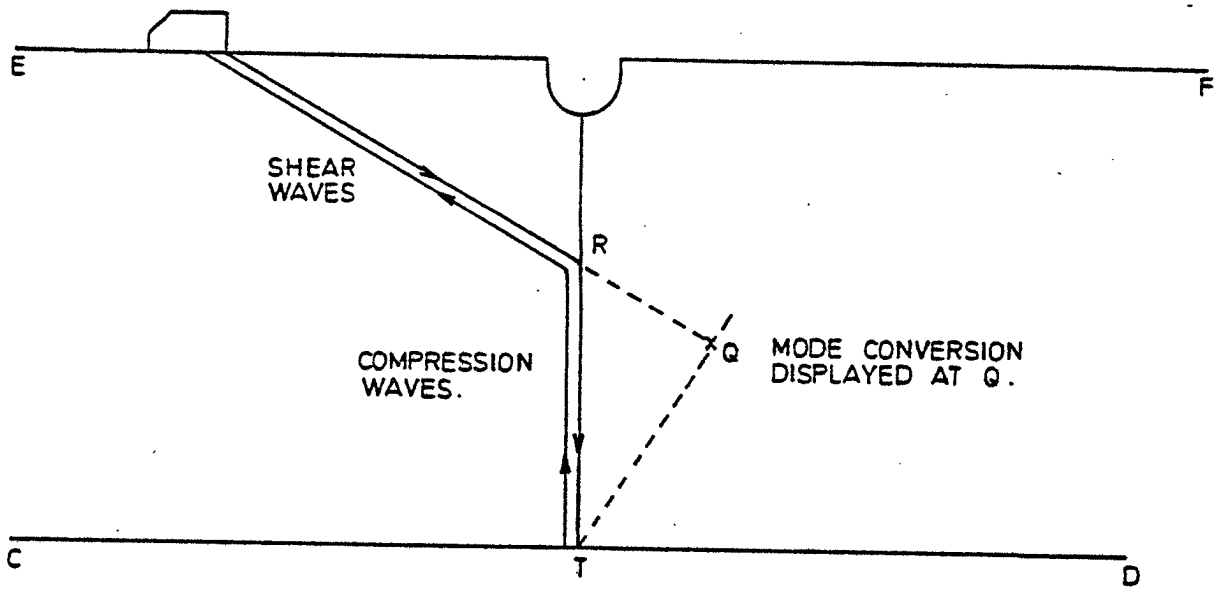

FIG.23(a). THE ORIGIN OF THE MODE CONVERSION SIGNALS WITH 60° PROBES.

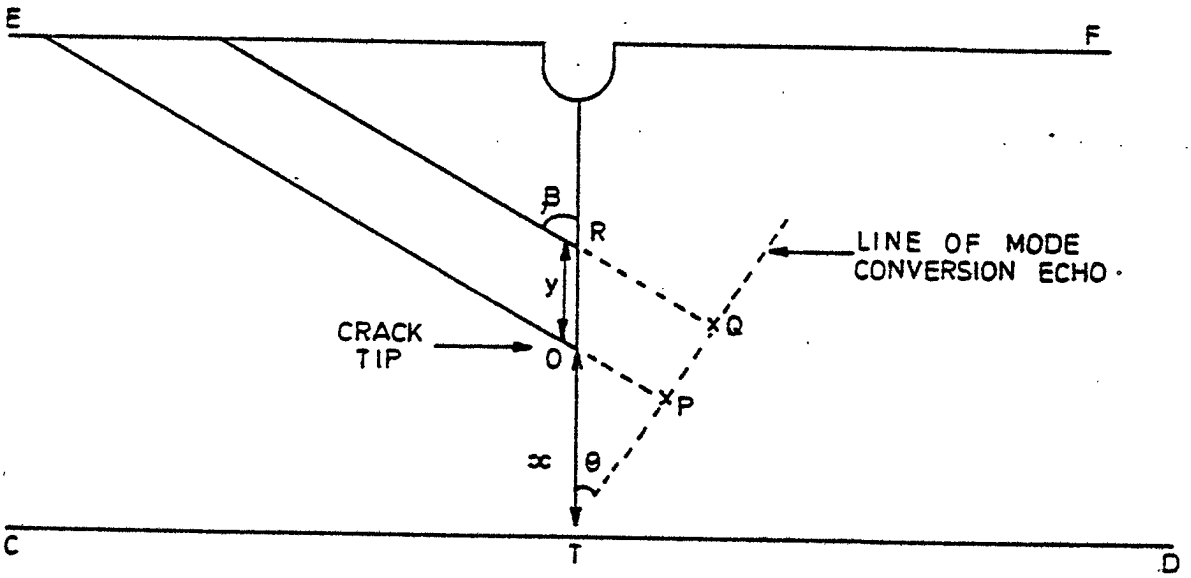

$$\frac{\text{VELOCITY OF COMPRESSION WAVES}}{\text{VELOCITY OF SHEAR WAVES}} = 1{\cdot}82$$

$\therefore$ SINCE $OP = \frac{x}{1{\cdot}82}$ AND $RQ = \frac{x+y}{1{\cdot}82}$, TRIANGLES OPT AND RQT ARE SIMILAR.

$\therefore$ THE MODE CONVERSION IS A STRAIGHT LINE AT AN ANGLE θ TO THE CRACK WHEN $\beta = 60°$, $\theta = 33{\cdot}3°$.

FIG.23(b). THE CONSTRUCTION OF THE MODE CONVERSION LINE BY THE B-SCAN

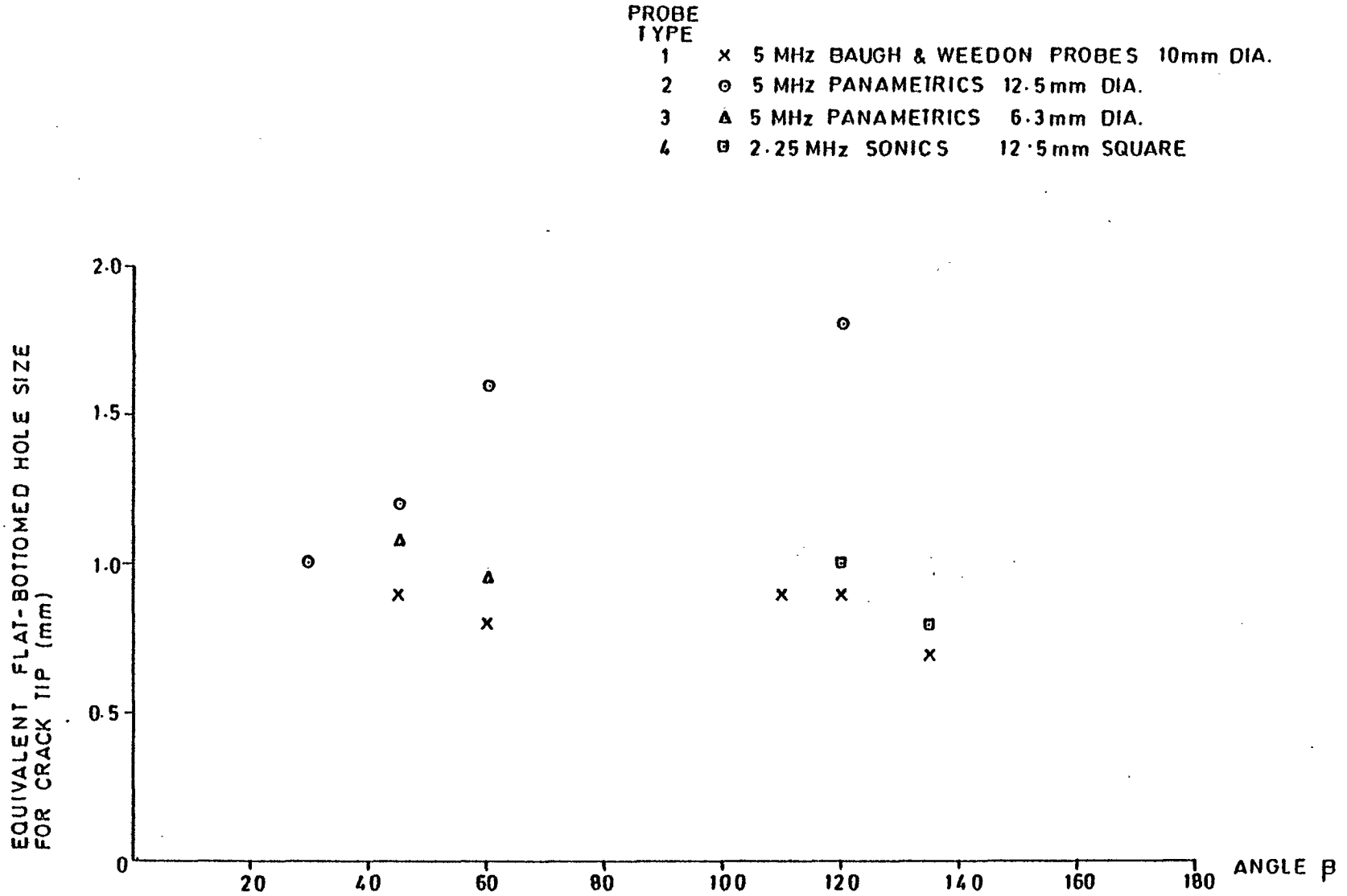

FIG.24 THE VARIATION OF THE CRACK TIP ECHO WITH ANGLE OF INCIDENCE (β) FOR SHEAR WAVES

PROBE ANGLE	x mm	y mm
45°	25	43
60°	45	70
70°	75	111

THE POSITION USED FOR EACH ANGLE OF PROBE

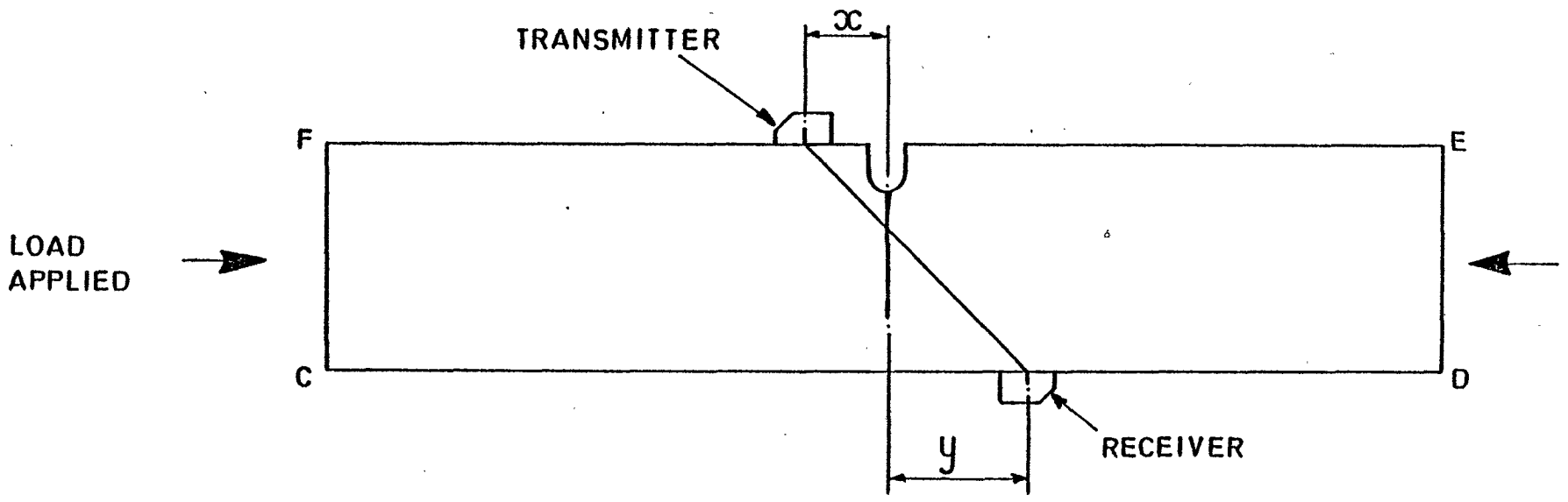

FIG. 25 EXPERIMENTAL ARRGT. USED TO MEASURE TRANSMISSION ACROSS THE CRACK

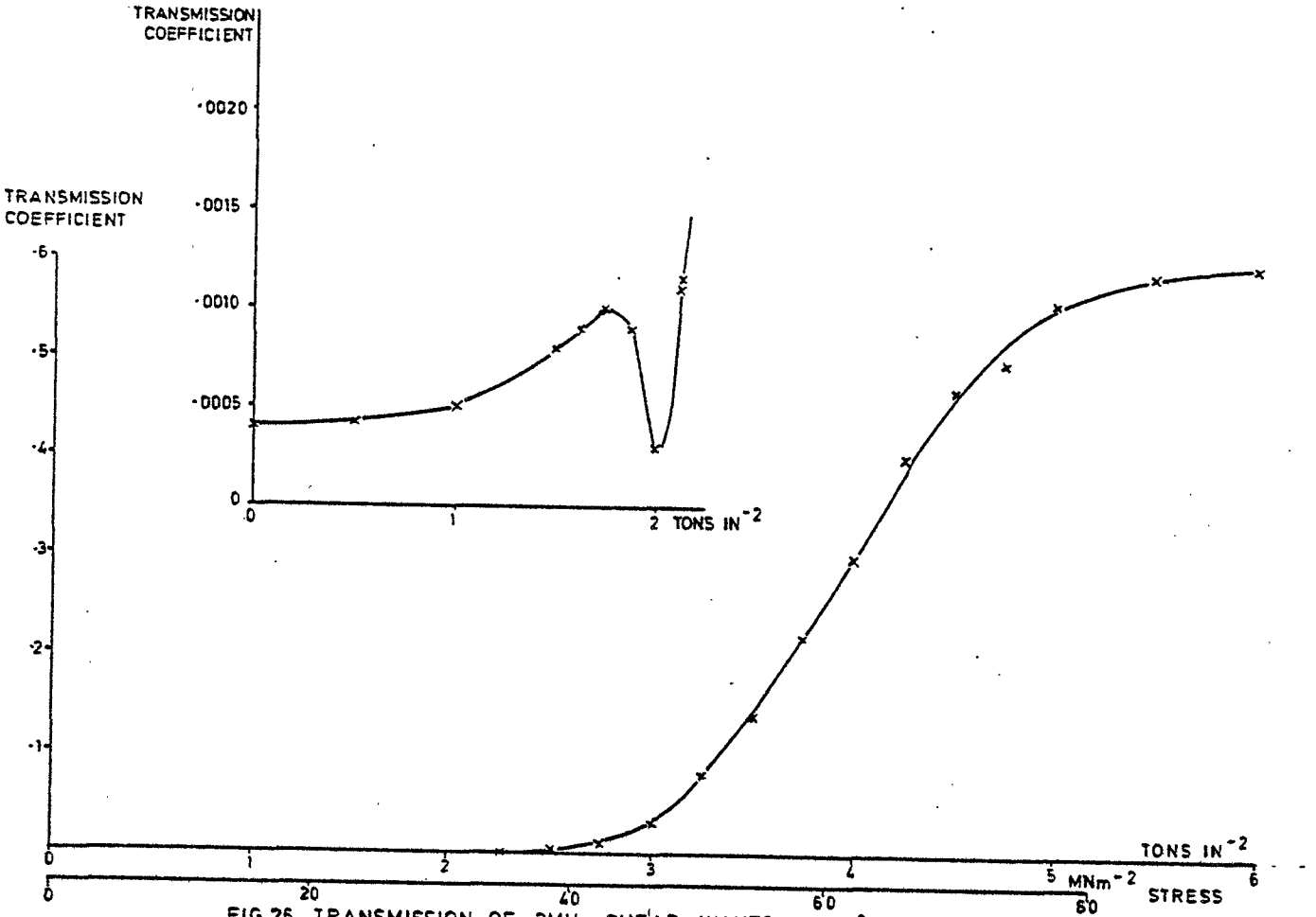

FIG.26 TRANSMISSION OF 2MHz SHEAR WAVES AT 45° TO THE CRACK

RC/SSR/AL/858

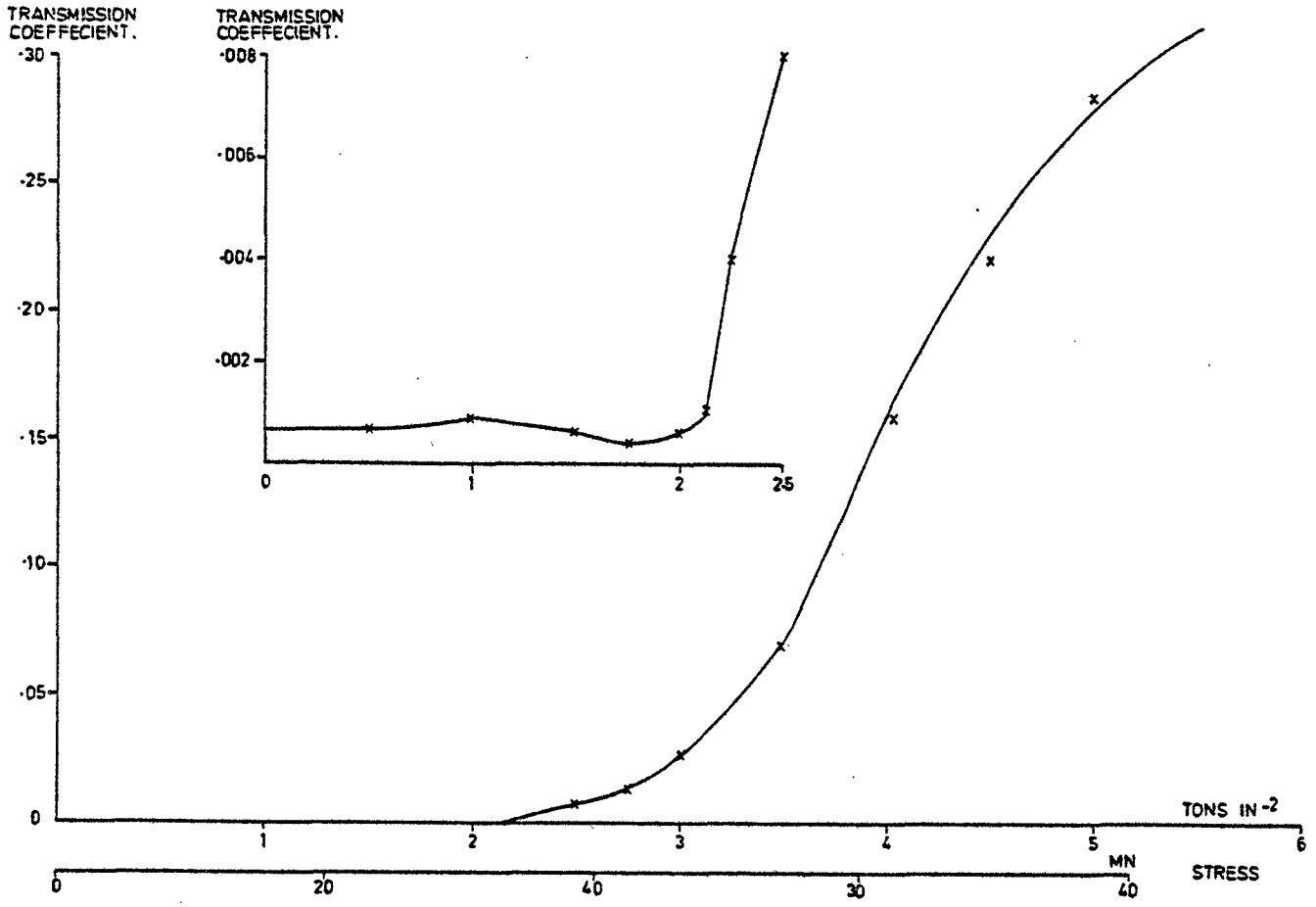

FIG 27 TRANSMISSION OF 5 MHz SHEAR WAVES AT 45° TO THE CRACK

RC/SSR/AL/859

MEAN STRESS APPLIED:- 80 MNm^{-2}

FLAW DETECTOR:- PA1020 TR MODE

PROBES:- BAUGH AND WEEDON - 2 MHz 15mm DIA. } SHEAR WAVE
5 MHz 10mm DIA. }

PROBE FREQUENCY	PROBE ANGLE	ANGLE OF INCIDENCE ON CRACK	TRANSMISSION THROUGH UNCRACKED BLOCK / TRANSMISSION THROUGH CRACK	TRANSMISSION COEFFICIENT
2 MHz	45°	45°	4 dB	0·6
	60°	30°	1 dB	0·9
5 MHz	45°	45°	10 dB	0·3
	60°	30°	9 dB	0·4

FIG. 28 COMPARISON OF TRANSMISSION THROUGH CRACKED AND UNCRACKED PARTS OF THE STEEL BLOCK

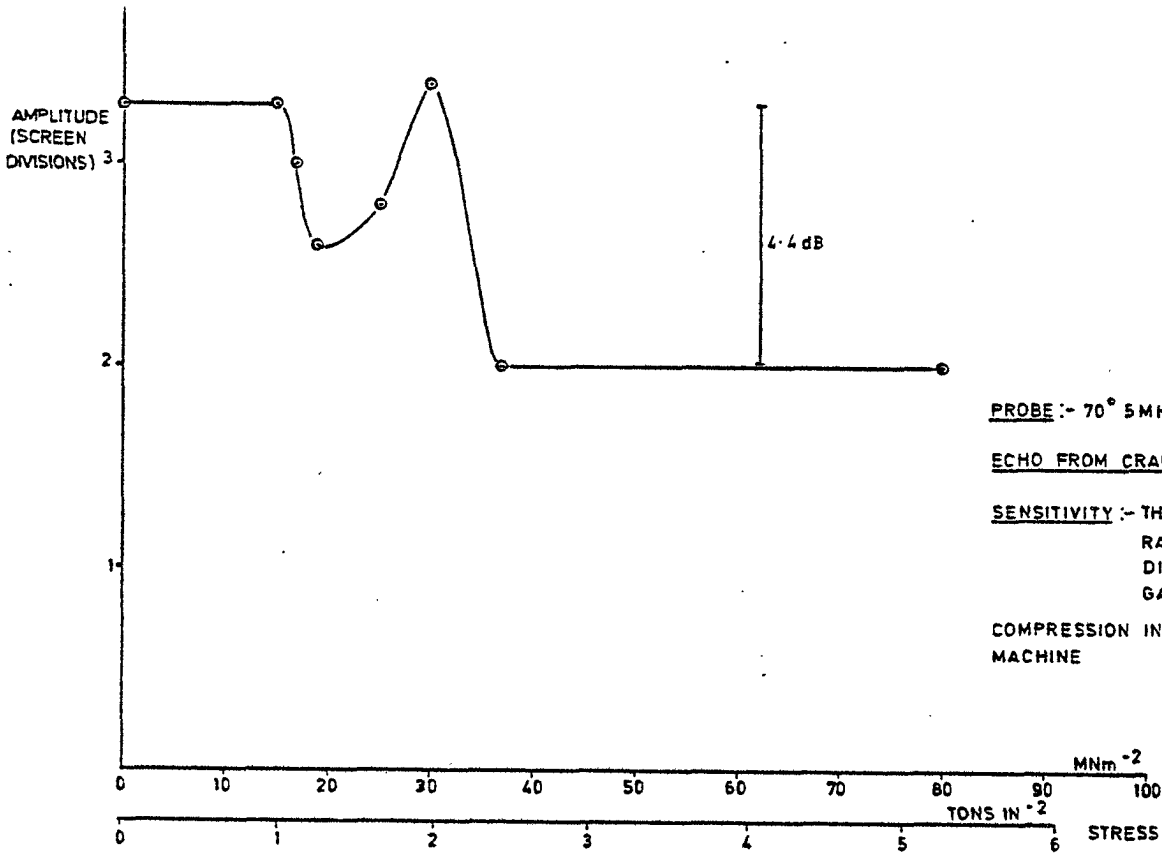

PROBE :- 70° 5MHz

ECHO FROM CRACK TIP DEPTH 23mm.

SENSITIVITY :- THE ECHO FROM A 50mm RADIUS EQUALS ONE DIVISION AT 48dB LESS GAIN

COMPRESSION IN THE MAND TEST MACHINE

FIG.29a REFLECTION OF 70° 5MHz SHEAR WAVES FROM THE CRACK TIP

RC/SSR/AL/8.6

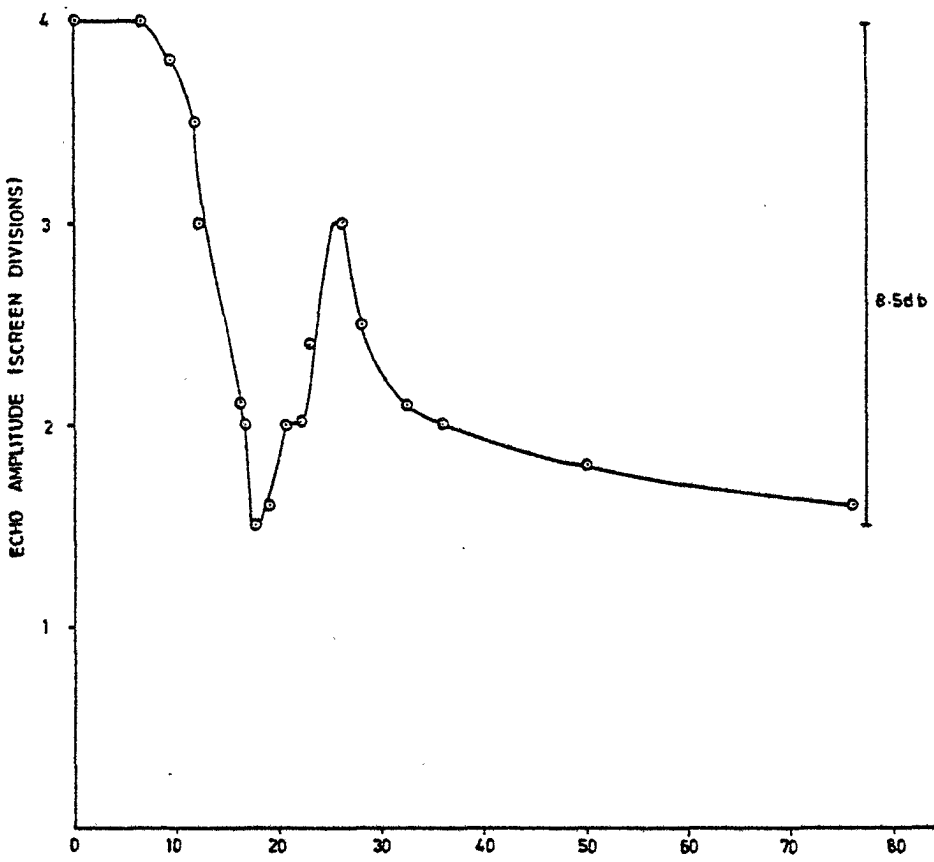

PROBE : 70° 5MHz

ECHO FROM CRACK TIP : DEPTH 23mm

SENSITIVITY : THE ECHO FROM A 50mm RADIUS EQUALS ONE DIVISION AT 48db LESS GAIN.

FIG 29(b) REFLECTION OF 70° 5 MHz SHEAR WAVES FROM THE CRACK TIP. COMPRESSION IN THE DENION TEST MACHINE.

RC/SSR/AL/8.7

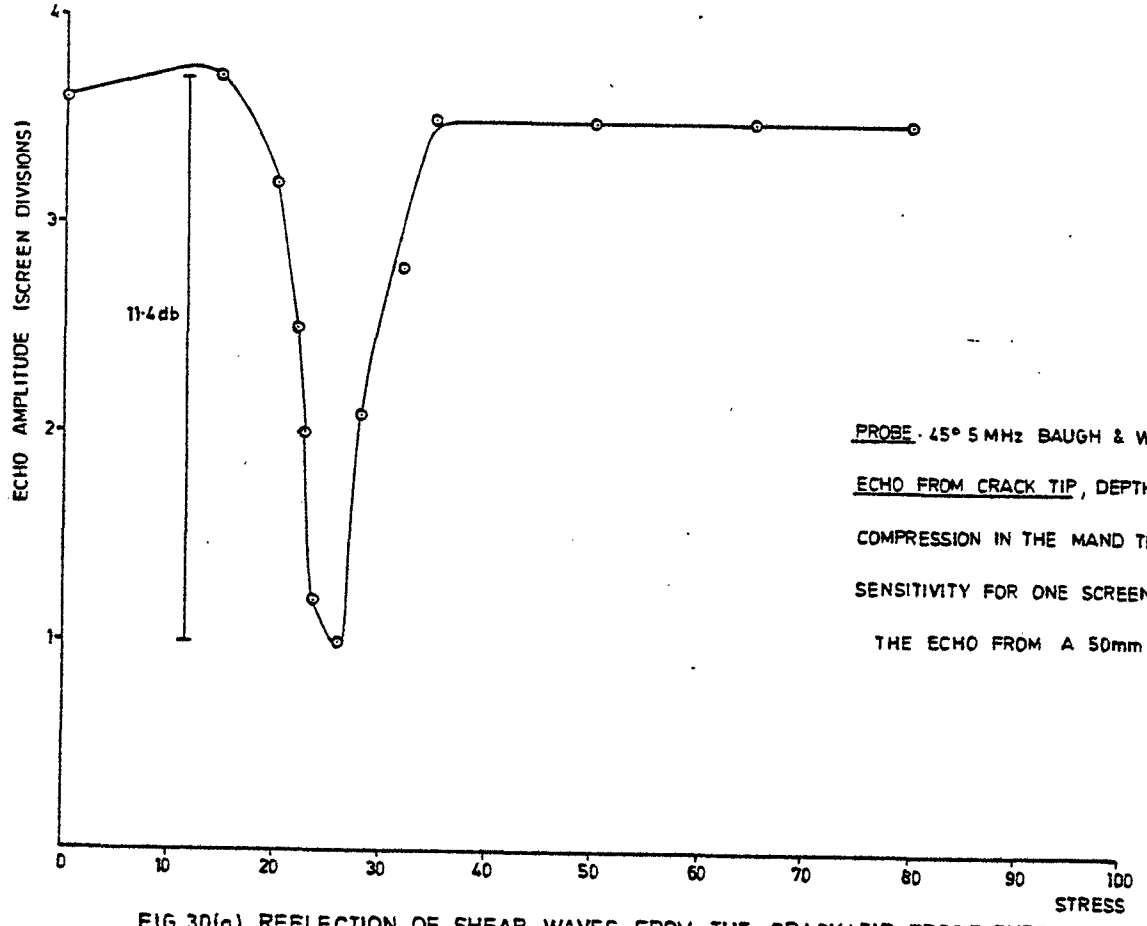

FIG 30(a) REFLECTION OF SHEAR WAVES FROM THE CRACK TIP. PROBE TYPE 1

RC/SSR/A4/959

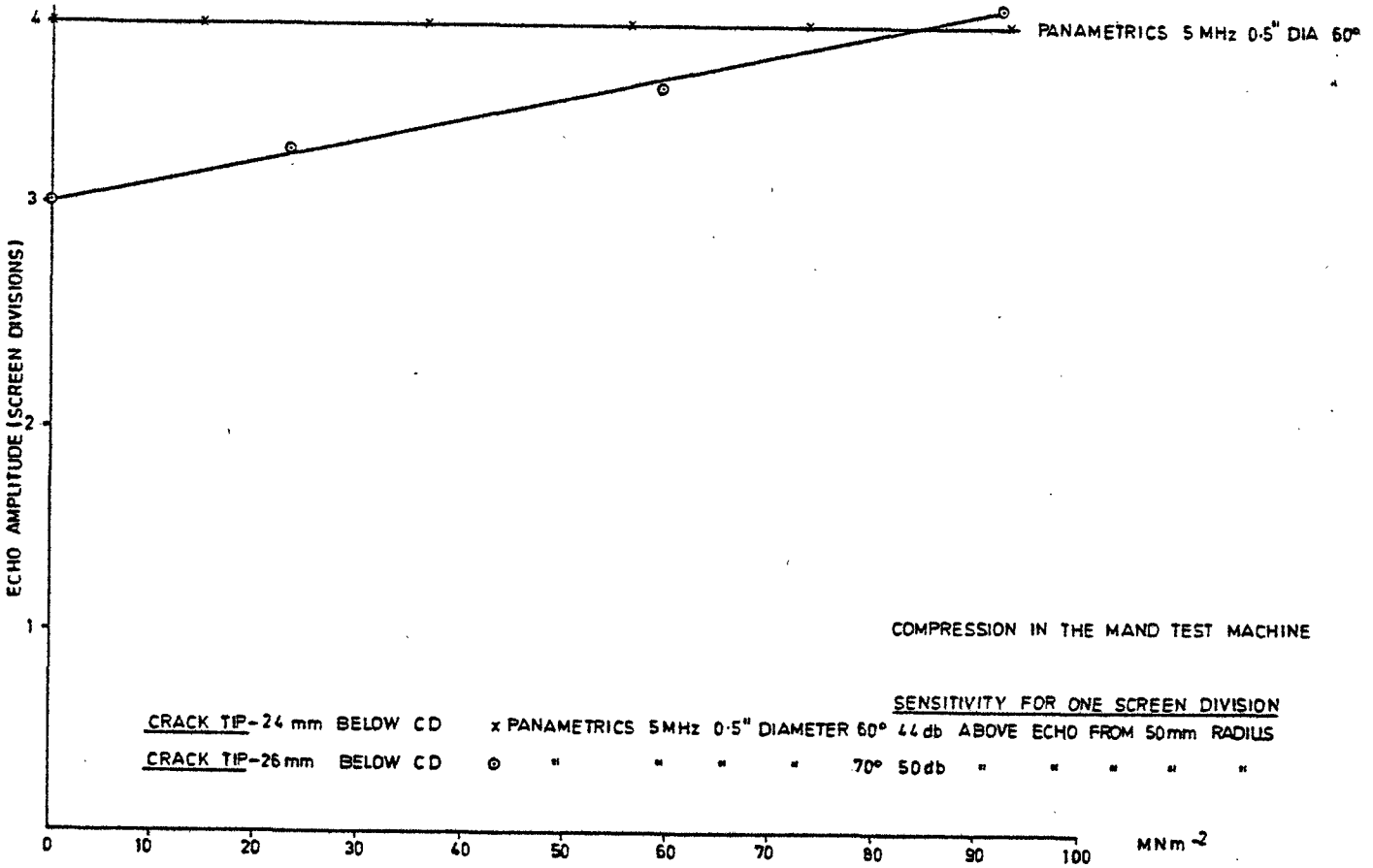

FIG.30(b). REFLECTION OF SHEAR WAVES FROM THE CRACK TIP.- PROBE TYPE 2

RC/SSR/A4/956

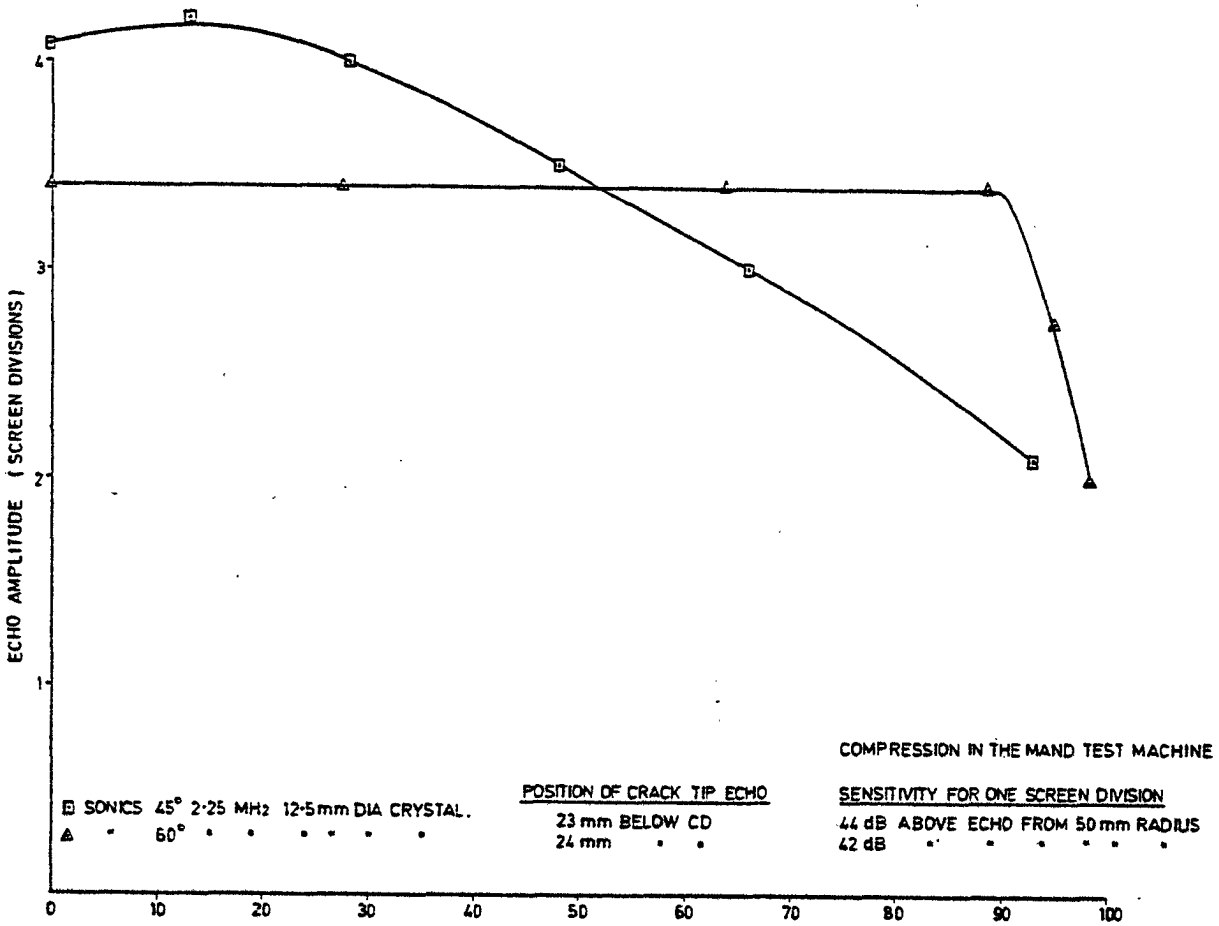

FIG. 30 (C). REFLECTION OF SHEAR WAVES FROM THE CRACK TIP – PROBE TYPE 4

RC/SSR/A4/963

	AVERAGE VALUES OF MAXIMUM CHANGES	MAXIMUM CHANGE	MINIMUM CHANGE
CRACK TIP	– 4·2 dB (10 READINGS)	– 11·4 dB	0·0 dB
CRACK FACE	– 1·9 dB (13 READINGS)	– 10·6 dB	0·0 dB

APPLIED STRESS :- 0→90 MNm^2

FIG.31. MAXIMUM, MINIMUM, AND AVERAGE VALUES OF CHANGES IN REFLECTIVITY WITH APPLIED STRESS.

RC/SSR/A4/965

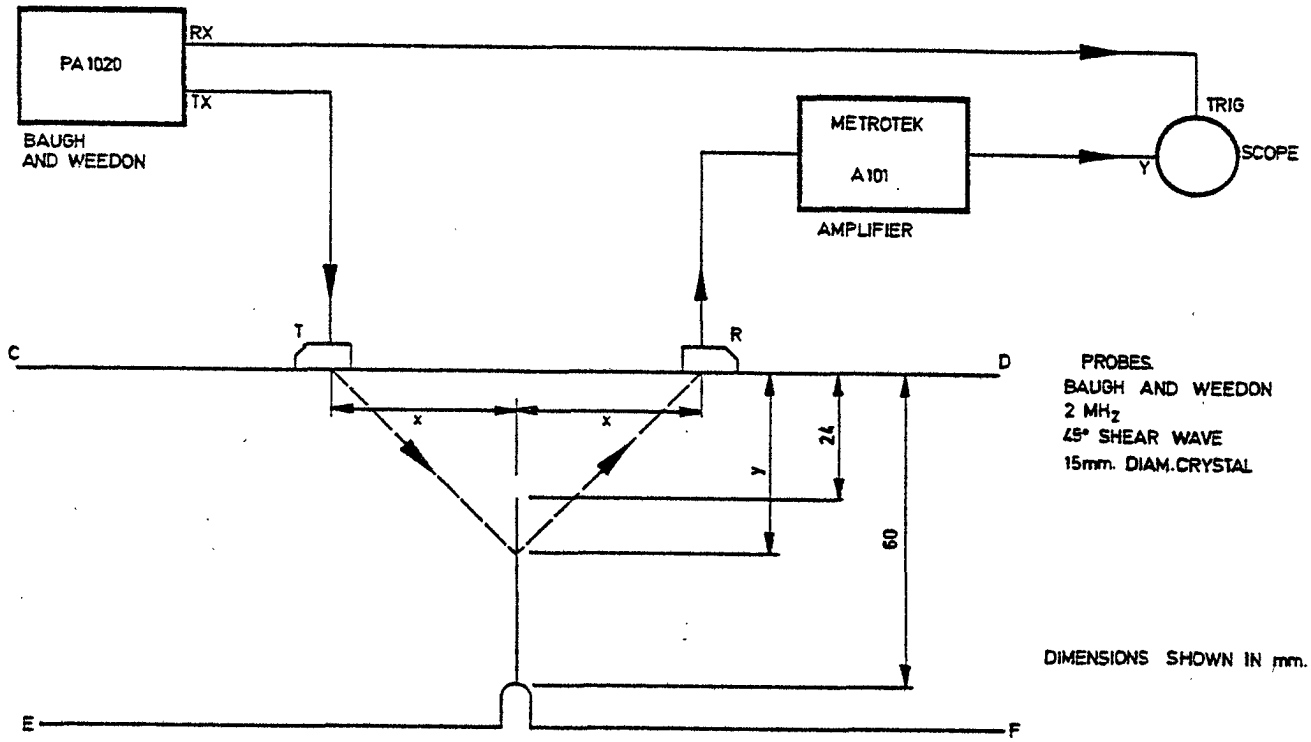

FIG. 32 EXPERIMENTAL CONFIGURATION FOR THE DIFFRACTION EXPERIMENTS.

RC/SSR/AL/962

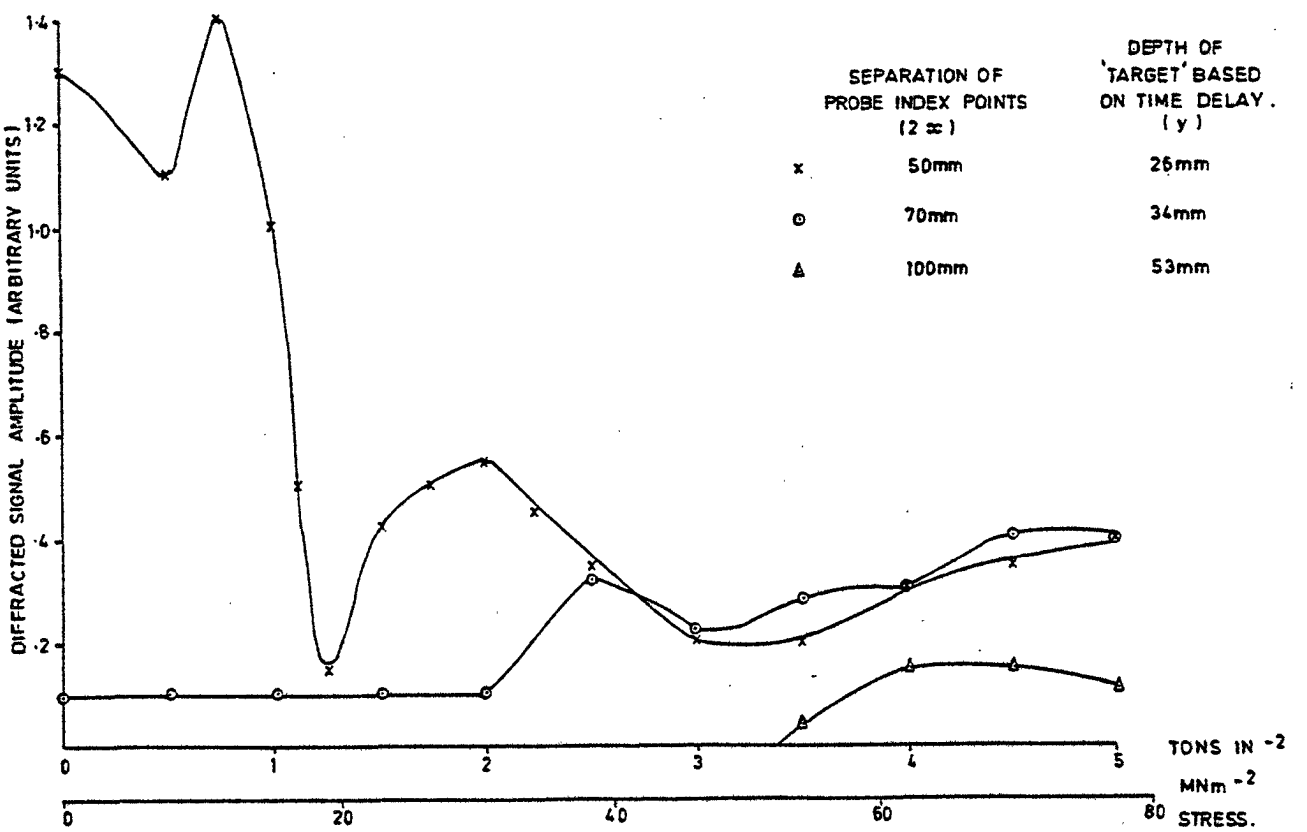

FIG 33 SIGNALS DIFFRACTED ACROSS THE FATIGUE CRACK AS A FUNCTION OF STRESS APPLIED.

RC/SSR/AL/964

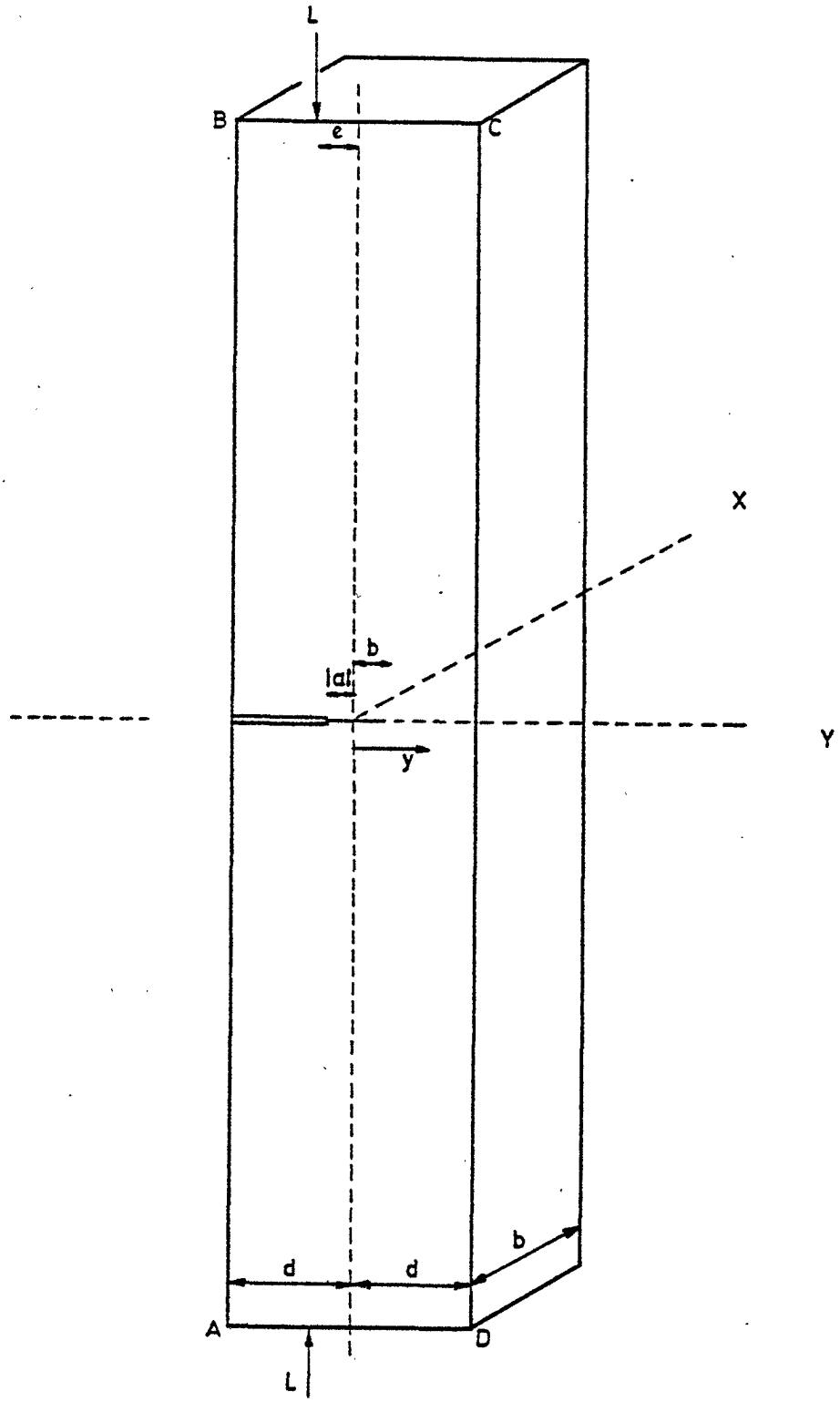

FIG. A1. A SIMPLIED DIAGRAM OF THE BLOCK USED TO CALCULATE THE STRESS DISTRIBUTION.

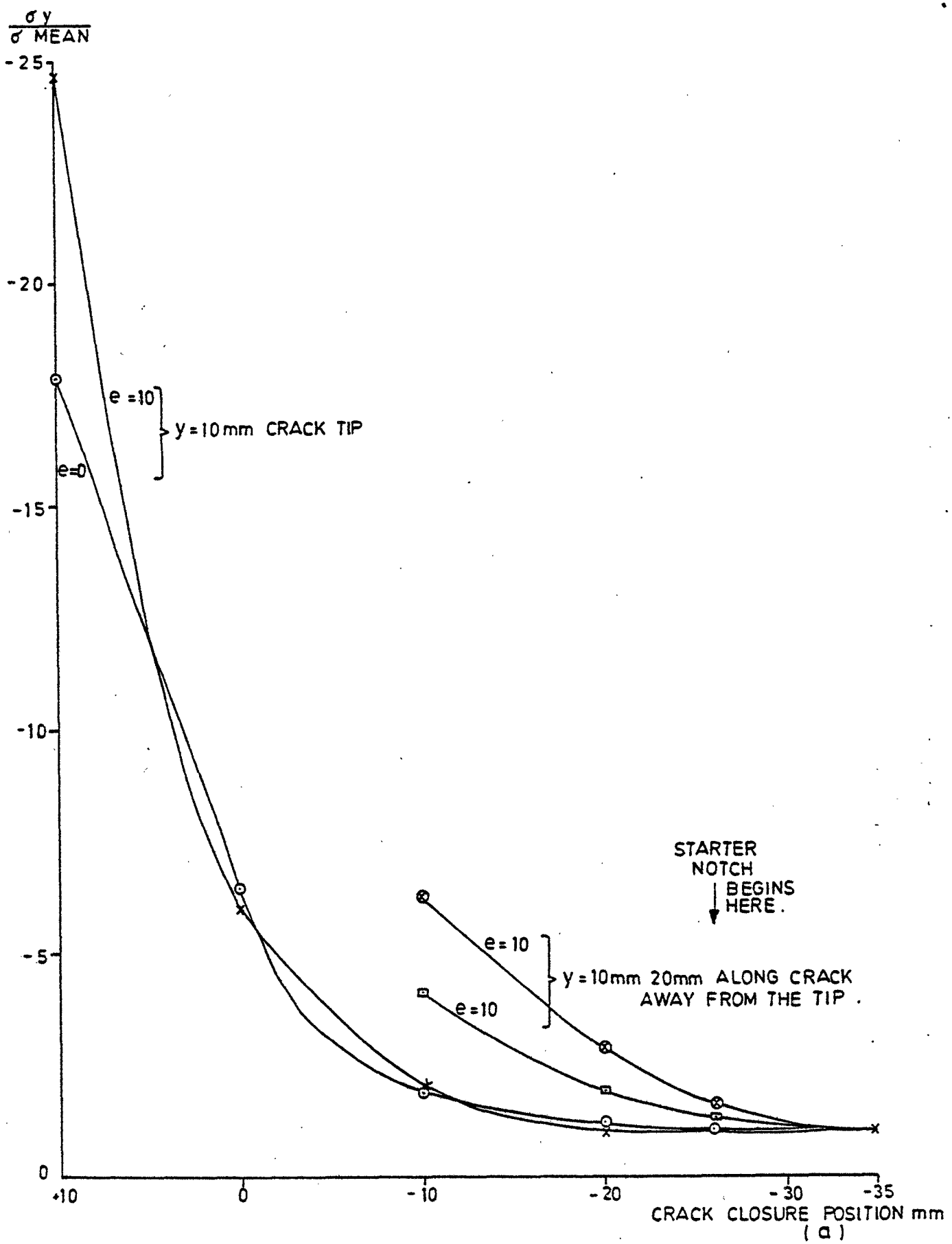

FIG A2 THE RATIO OF LOCAL STRESS TO MEAN STRESS AS THE CRACK CLOSES.